CANCER

EGFR targeting PhosTACs as a dual inhibitory approach reveals differential downstream signaling

Zhenyi Hu[1,2]†, Po-Han Chen[1,3,4]†, Wenxue Li[5]†, Mackenzie Krone[1], Sijin Zheng[1], Jacques Saarbach[1], Ines Urquizo Velasco[1], John Hines[1], Yansheng Liu[5], Craig M. Crews[1,6,7,8]*

We recently developed a heterobifunctional approach [phosphorylation targeting chimeras (PhosTACs)] to achieve the targeted protein dephosphorylation (TPDephos). Here, we envisioned combining the inhibitory effects of receptor tyrosine kinase inhibitors (RTKIs) and the active dephosphorylation by phosphatases to achieve dual inhibition of kinases. We report an example of tyrosine phosphatase–based TPDephos and the effective epidermal growth factor receptor (EGFR) tyrosine dephosphorylation. We also used phosphoproteomic approaches to study the signaling transductions affected by PhosTAC-related molecules at the proteome-wide level. This work demonstrated the differential signaling pathways inhibited by PhosTAC compared with the TKI, gefitinib. Moreover, a covalent PhosTAC selective for mutated EGFR was developed and showed its inhibitory potential for dysregulated EGFR. Last, EGFR PhosTACs, consistent with EGFR dephosphorylation profiles, induced apoptosis and inhibited cancer cell viability during prolonged PhosTAC treatment. PhosTACs showcased their potential of modulating RTKs activity, expanding the scope of bifunctional molecule utility.

INTRODUCTION

Epidermal growth factor receptor (EGFR) belongs to the ErbB family of receptor tyrosine kinase (TK) proteins (*1*). EGFR is composed of an extracellular ligand binding domain, a transmembrane domain, and an intracellular kinase domain (*2*, *3*). Upon ligand binding by epidermal growth factor (EGF), tumor necrosis factor–α (TNF-α), etc., EGFR forms homodimers or heterodimers with other ErbB family receptors, which then leads to a conformational change and subsequent activation of TK domains (*4*).

Activated EGFR promotes downstream signal transduction through autophosphorylation on multiple sites. The tyrosine residue phosphorylation at the EGFR C-terminal tail provides docking sites for proteins with Src Homology (SH2) and phosphotyrosine-binding (PTB) domains (*5*, *6*) such as the adaptor proteins SHC-transforming protein 1 (SHC) and growth factor receptor-bound protein 2 (Grb2) (*7*, *8*). For example, EGFR phospho-Y974 (pY974) has been shown to recruit SHC, signal transducer and activator of transcription 5 (STAT5), and Src, while EGFR pY1173 binds to Grb2, SHC, phospholipase C gamma 1, and Src homology region 2 domain-containing phosphatase-1 (*9*). In addition to these auto-phosphorylated tyrosine sites, phosphorylation of Y845 of EGFR, located within the activation loop of the kinase domain, correlates with EGF-dependent activation of EGFR (*10*–*12*).

EGFR phosphorylation initiates multiple downstream signaling pathways, including the mitogen-activated protein kinases (MAPKs), phosphoinositide 3-kinases/protein kinase B (also known as AKT), and the Janus kinase (JAK)/STAT pathway (*1*), and accordingly affects several fundamental cellular processes, such as cell proliferation, cell metabolism, and survival (*13*). Phosphorylated EGFR activates MAPK pathway through adaptors proteins such as GRB2 and son of sevenless homolog 1 (SOS1), promoting cell growth and proliferation (*14*). In addition, EGFR can directly activate STAT3 or through Src and JAK–STAT3, which can then dimerize and translocate into nucleus, where it can promote cell differentiation, survival, and proliferation (*15*).

EGFR dysregulation has been implicated in pathologies of many different types of cancers. In particular, EGFR amplification, overexpression, and mutations have been frequently found in non–small cell lung cancer (*16*, *17*). To address EGFR's critical role in cancer pathology, many tyrosine kinase inhibitors have been developed, such as the first-generation TK inhibitors (TKIs) (gefitinib), second-generation TKI (afatinib), and third-generation TKI (osimertinib) (*18*). While these TKIs have improved cancer therapeutic intervention, unfortunately, resistance inevitably emerges after long-term use. For instance, EGFR T790M leads to gefitinib resistance through enhancing EGFR's affinity toward adenosine triphosphate (ATP) and/or blocking of gefitinib binding (*19*, *20*), and C797S mutation renders osimertinib ineffective through replacement of the osimertinib-reactive cysteine residue (*21*). In addition, TKIs are often associated with a number of undesirable side effects, namely, dermatological adverse events such as pruritus and acneiform skin rashes (*22*–*24*). These inadequacies of TKIs drive continued interest in therapeutic avenues for EGFR inhibition.

Because phosphorylation is critical for EGFR activation and downstream signal transduction, induced EGFR dephosphorylation provides a promising avenue for an alternative approach to EGFR inhibition. Phosphatases are a group of enzymes that function by removing phosphates from phosphorylated proteins, thereby regulating their function. Phosphatases are categorized into several classes: phosphoprotein phosphatases (PPPs), Mg^{2+}/Mn^{2+}-dependent protein phosphatases (PPMs), protein tyrosine phosphatases (PTPs), and aspartate-based protein phosphatases (*25*). Among them, PTPs selectively remove phosphate groups from tyrosine residues and have been

[1]Department of Molecular, Cellular, and Developmental Biology, Yale University, New Haven, CT 06511, USA. [2]Interdisciplinary Research Center on Biology and Chemistry, Shanghai Institute of Organic Chemistry, Chinese Academy of Sciences, Shanghai 201210, China. [3]Department of Biochemistry and Molecular Biology, College of Medicine, National Cheng Kung University, Tainan City, 701, Taiwan. [4]Institute of Basic Medical Sciences, College of Medicine, National Cheng Kung University, Tainan City, 701, Taiwan. [5]Yale Cancer Biology Institute, Yale University, West Haven, CT 06516, USA. [6]Department of Chemistry, Yale University, New Haven, CT 06511, USA. [7]Department of Pharmacology, Yale University, New Haven, CT 06511, USA. [8]Yale University School of Medicine, New Haven, CT 06511, USA.
*Corresponding author. Email: craig.crews@yale.edu
†These authors contributed equally to this work.

shown to play important roles in regulating receptor or nonreceptor tyrosine kinases. For instance, protein tyrosine phosphatase nonreceptor type 2 (PTPN2) has been reported to regulate EGFR function through its dephosphorylation (*26*, *27*).

While phosphatases have critical roles in regulating cellular homeostasis and immense potential in disease treatment, their clinical application has been insufficiently explored (*28*, *29*). Recent advances in bifunctional molecules, however, provide a paradigm shift in drug development. Unlike traditional small-molecule enzyme inhibitors that function through an occupancy-driven mechanism, heterobifunctional molecules function via event-driven mechanisms. Proteolysis targeting chimera (PROTAC), first developed by our laboratory, is a prime example of a bifunctional molecule in that they have demonstrated advantages over traditional inhibitors, such as a catalytic mode of action (*30*), high selectivity (*31*), and extended period of effect (*32*, *33*). Similar to PROTACs, we have more recently reported phosphorylation targeting chimeras (PhosTACs) as an approach to modulate phosphorylation of proteins of interest (POIs) (*34*, *35*), which specifically and significantly induced targeted protein [i.e., programmed cell death protein 4 (PDCD4), forkhead box O3 (FOXO3), and tau] dephosphorylation. In addition, Zheng *et al.* (*36*), Yamazone *et al.* (*37*), and Zhang *et al.* (*38*) used bifunctional molecules to achieve dephosphorylation of tau, AKT, and apoptosis signal–regulating kinase 1 (ASK1), respectively. However, all aforementioned works are based on serine/threonine phosphatases, and the potential of tyrosine phosphatase (especially against RTKs) has not been investigated.

In this study, we envisioned combining the "occupancy-driven modality" of TKIs with the "event-driven modality" of bifunctional molecules to achieve dual inhibition of EGFR with TKI-based PhosTAC. We report an example of harnessing a tyrosine phosphatase (PTPN2) to dephosphorylate EGFR. As a proof of concept, we showed that PhosTACs dephosphorylate wild type (WT) and mutated EGFR (L858R/T790M) in HeLa cells and H1975 cells, respectively, which subsequently inhibited cellular proliferation. Moreover, we used the phosphoproteomic method to study the signaling transductions affected by PhosTAC at the proteome-wide level. Site-specific phosphoproteomic data confirmed the induced EGFR dephosphorylation by PhosTACs, and its differential influence on cell signaling pathways compared with the EGFR inhibitor, gefitinib. Given that TKIs are widely used as a major treatment for cancer-targeted therapy, we believe that this technology has the potential as a modality for both basic and translational research.

RESULTS

PhosTACs recruit tyrosine phosphatase via a fusion protein system

Given its well-established significance in cancer pathology, we selected EGFR as the target protein to explore the potential of tyrosine phosphatase recruitment using PhosTACs (Fig. 1A). We used the first-generation EGFR inhibitor, gefitinib, as the EGFR recruiting molecule because it has high affinity ($K_d = 35$ nM) toward WT EGFR (*20*). Because of the lack of well-established tyrosine phosphatase activator, we used the FK506 binding protein 12 ($FKBP12^{F36V}$) fusion protein strategy as previously described (*34*). In this way, this fusion protein can be easily recruited with $FKBP12^{F36V}$ small-molecule ligand (*39*), providing an efficient bio-orthogonal method that has been widely used in PROTAC research and proven to be an effective chemical biology tool (*40*, *41*). We chose the 45-kDa isoform of PTPN2 (TC45), a phosphotyrosine-specific nonreceptor phosphatase, as the phosphatase for the EGFR to minimize possible target protein incompatibility. The PTPN2-TC45 was fused with $FKBP12^{F36V}$ tag protein at its N-terminal and stably expressed in HeLa cells as we previously did for protein phosphatase 2A (PP2A) (*34*). Last, to construct the bifunctional PhosTACs, we used chemical linkers to connect the $FKBP12^{F36V}$ ligands and gefitinib molecule and established a small library of PhosTACs (Fig. 1B and figs. S1, A and B and S2; including GePhos1, GePhos3, GePhos6, and GePhos9).

Because this PhosTAC was designed to combine the inhibitory effects of both a TKI and active dephosphorylation by a phosphatase, it is intriguing to distinguish between any dephosphorylation effects attributable to the gefitinib molecule alone versus that from the active PTPN2 recruitment. To distinguish these two effects, we designed a nonbinding PhosTAC-negative control inspired by inactive epimers in PROTAC development (*42*). PROTAC epimers have similar physical and chemical properties as active PROTACs but cannot recruit E3 ligases, leading to no POI degradation (*43*). Similarly, we designed a GePhos1 epimer that lacks binding affinity toward $FKBP12^{F36V}$. The FKBP12 protein is a rotamase that catalyzes the cis-transisomerization of L-prolyl amide bonds (*44*), and the S-pipecolic ester motif in $FKBP12^{F36V}$ ligand was shown to be the main contributor for binding (Fig. 1B and fig. S1A, circled in red) (*45*). Therefore, we hypothesized that inversion of the stereocenter of pipecolic ester motif may lead to decreased binding affinity. Accordingly, the $FKBP12^{F36V}$ epimer ligand with an R-pipecolic ester motif was synthesized, and its binding affinity for recombinant $FKBP12^{F36V}$ was measured (fig. S1, B and C) by surface plasmon resonance (SPR) and isothermal titration calorimetry (ITC). As expected, we observed a low nanomolar K_d for binding of the original $FKBP12^{F36V}$ ligand to $FKBP12^{F36V}$ ($K_d = 16$ nM), and none for the epimer by single- or multi-cycle SPR (Fig. 1C and fig. S3, A and B), which was corroborated by ITC ($K_d = 9.9 \pm 7.8$ nM) (fig. S3C). Moving forward, we used this epimer ligand to generate an inactive GePhos1 epimer (denoted iGePhos1) as a nonbinding negative control (Fig. 1B). As iGephos1 lacks the phosphatase recruiting possibility, thus any possible dephosphorylation effect induced by iGephos1 could be attributed to the residual effect of the gefitinib molecule. As expected, we observed enhanced ternary complex formation induced by GePhos1 (fig. S22). It is worth noting that $FKBP12^{F36V}$ fusion protein has been widely used as a tool in PROTAC studies (*46*), cell imaging (*47*), etc., this epimer compound provides a valuable negative control compound for future chemical biology studies.

PhosTAC induces dephosphorylation in a catalytic manner

One of the advantages of bifunctional molecules, exemplified by PROTACs, is its unique event-driven pharmacology model (*33*), executing catalytical effect (*48*). As phosphorylation is fast and reversible, we hypothesize that PhosTAC may also have similar catalytic potential that phosphate groups decorated on EGFR can be removed by PhosTAC-recruited PTPN2 (Fig. 1A), in an iterative fashion. To test the catalytic mechanism of PhosTACs, we monitored the amount of released phosphate with the malachite green, which can form complex with free orthophosphate and can be detected by a spectrophotometer with absorbance at 620 nm. We co-incubated recombinant proteins of the EGFR kinase domain and $FKBP12^{F36V}$-PTPN2 with GePhos1 or iGePhos1, respectively, in vitro. After 1 hour of reaction, iGePhos1 did not induce significant phosphate release enhancement

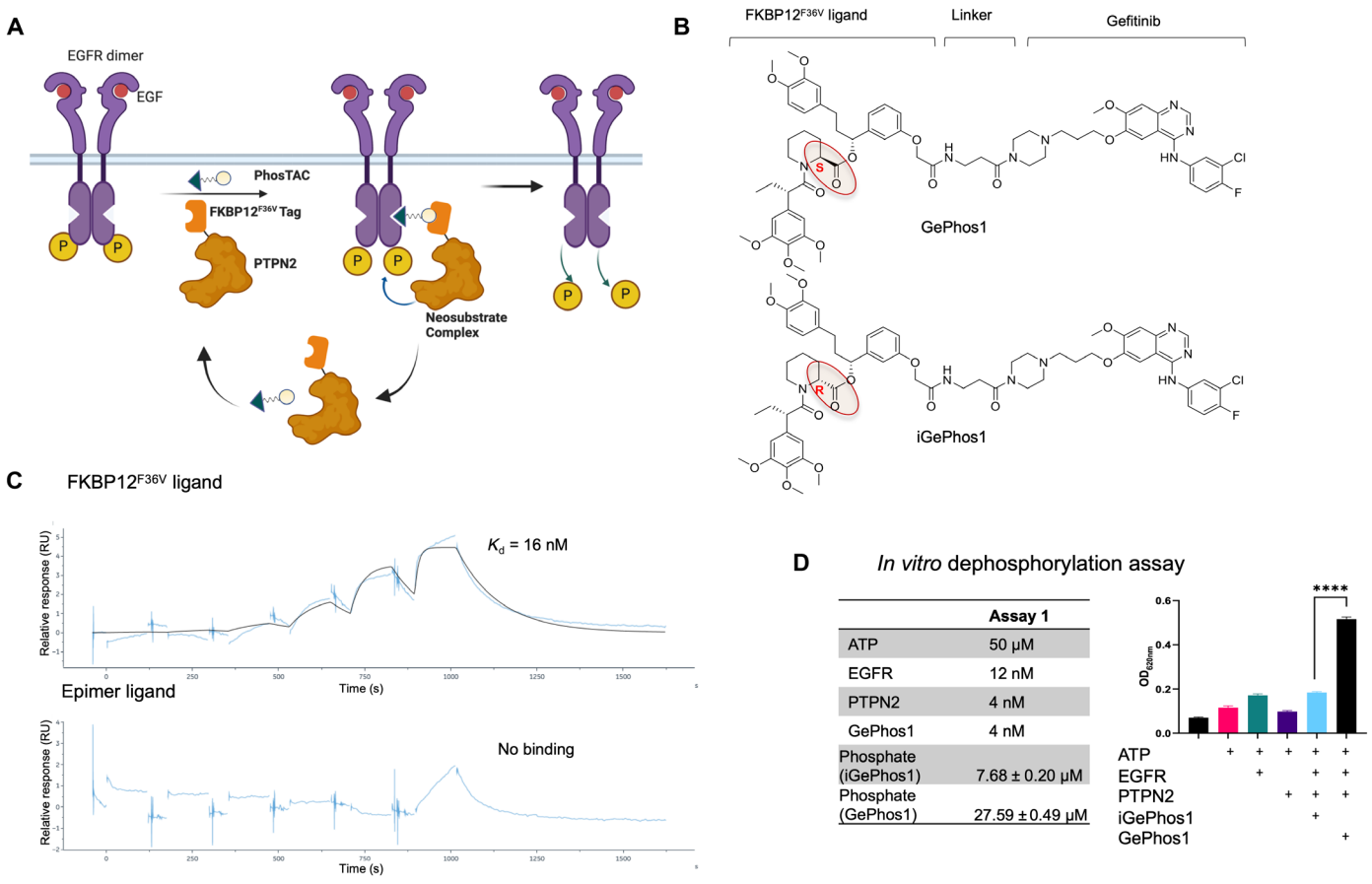

Fig. 1. Design of EGFR-targeting PhosTACs. (**A**) Scheme of the EGFR PhosTAC action mechanism. (**B**) Structure of GePhos1 and iGePhos1. (**C**) SPR sensograms of FKBP12^{F36V} binding to FKBP12^{F36V} ligand (top) and FKBP12^{F36V} epimer ligand (bottom). FKBP12^{F36V} protein exhibited high affinity toward FKBP12^{F36V} ligand (K_d =16 nM), while no notable binding was detected for FKBP12^{F36V} epimer ligand. (**D**) Catalytic dephosphorylation effect of PhosTACs. EGFR, PTPN2, and PhosTACs were incubated with the indicated condition for 1 hour. The dephosphorylation effects were monitored via phosphate release as indicated by OD_{620} nm in the Malachite Green assay.

compared with EGFR or PTPN2 protein alone in ATP solution, while GePhos1 induced a significantly higher amount of phosphate release compared to the iGePhos1 (Fig. 1D). We observed that the released phosphate induced by GePhos1 was 27.59 ± 0.49 μM compared with 7.68 ± 0.20 μM by iGePhos1, which was several thousand times equivalent of PhosTAC and PTPN2. Similar results were also obtained with lower amount of EGFR, PTPN2, or PhosTAC molecules in vitro (fig. S4). This result is in accordance with the PTPN2's high catalytic activity (*49*), showcasing the catalytic effect of PhosTAC. Previously, our laboratory reported the catalytic effect of PROTAC (*48*), demonstrating that one PROTAC can induce the installation of multiple ubiquitin with the stoichiometry of about three, and the higher catalytic rate of PhosTAC indicates potential for kinase inhibition.

PhosTAC (GePhos1) induces EGFR dephosphorylation

Next, we tested the ability of EGFR PhosTACs to induce intracellular EGFR dephosphorylation in a FKBP12^{F36V}-PTPN2(TC45)–engineered HeLa cells. In this engineered cell line, we observed slightly reduced cell growth compared with the parental HeLa cells (fig. S5). We hypothesized that serum starvation would arrest and synchronize randomly activated EGFR in regular culture conditions, so HeLa cells with WT EGFR stably expressing FKBP12^{F36V}-PTPN2(TC45) were serum-starved for 24 hours. In addition, because EGFR phosphorylation cycle is rapid and short (less than 20 min based on our data), PhosTAC may not act in time without pretreatment. Thus, serum starvation and PhosTAC cotreatment were applied in our experiments. After which, cells were subsequently stimulated with EGF (100 ng ml^{-1}) for 15 min, collected and lysed, and then analyzed via immunoblotting. We tested the ability of EGFR PhosTACs to induce intracellular EGFR dephosphorylation. Among the PhosTACs (with different linker length) tested, GePhos1 demonstrated the optimal potency (fig. S6); thus, we next focused on the investigation of GePhos1. Relative to treatment with dimethyl sulfoxide (DMSO) or iGePhos1, cells treated with 100 nM GePhos1 displayed profound EGFR dephosphorylation at both EGFR pY1068, which is one of the major EGFR autophosphorylation sites, and at pY845, a key site within the kinase loop (Fig. 2A, figs. S7 and S8). Because EGFR phosphorylation at the C-terminal tail is crucial for the recruitment and activation of downstream signaling proteins, we also analyzed the phosphorylation state of proteins known to associate with activated EGFR. As shown in Fig. 2A, notable dephosphorylation of STAT3 pY705 was observed in GePhos1-treated

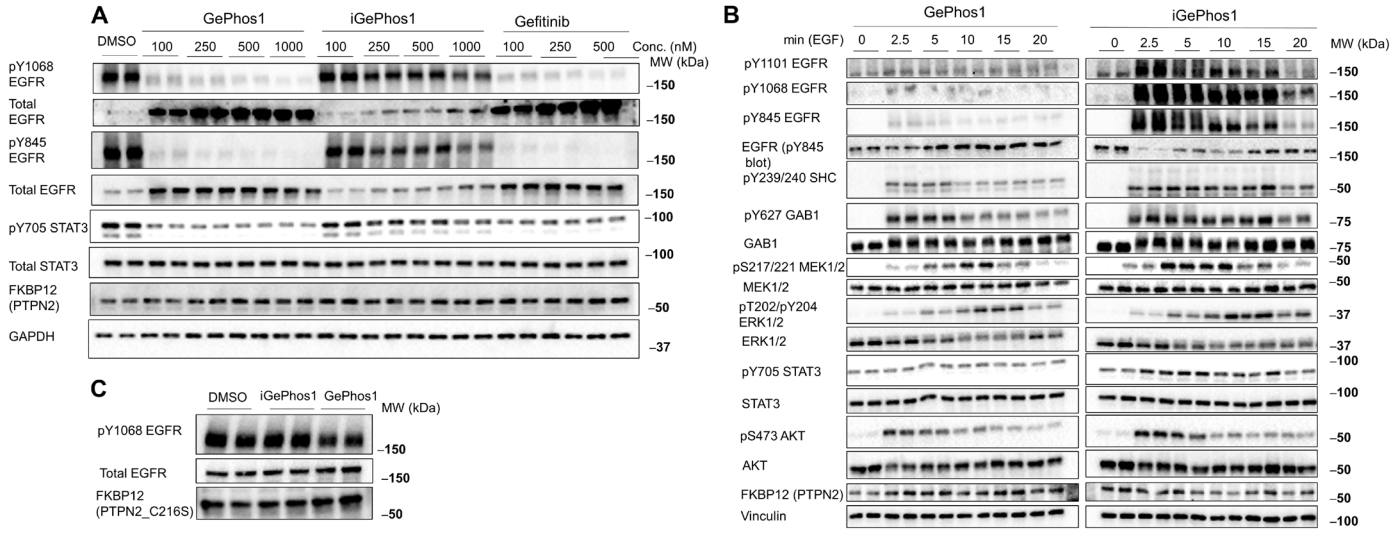

Fig. 2. EGFR PhosTAC (GePhos1) induced dephosphorylation. (**A**) PhosTAC induced dephosphorylation in FKBP12^{F36V}-PTPN2 cell line. FKBP12^{F36V}-PTPN2 HeLa cells were treated with indicated concentrations of DMSO, GePhos1, iGePhos1, and gefitinib for 24 hours under serum-free conditions, followed by treatment with EGF (100 ng ml^{-1}) for 15 min. Cell lysates were collected and analyzed by Western blot using indicated antibodies. (**B**) PhosTAC induced rapid dephosphorylation. FKBP12^{F36V}-PTPN2 HeLa cells were treated with 500 nM GePhos1 and iGePhos1 for 24 hours under serum-free conditions, followed by treatment with EGF (100 ng ml^{-1}) for indicated times; 0 min indicated no EGF treatment. Cell lysates were collected analyzed by Western blot using indicated antibodies. (**C**) PhosTAC-induced dephosphorylation was compromised in the PTPN2-C216S enzymatic-dead cell line. FKBP12^{F36V}-PTPN2^{C216S} HeLa cells were treated with 500 nM GePhos1 and iGePhos1 for 24 hours, followed by treatment with EGF (100 ng ml^{-1}) for 15 min. Cell lysates were collected and analyzed by Western blot using indicated antibodies. EGFR and FKBP12 were used as the normalization and loading control, respectively, for pY1068 EGFR. Representative data of four replicates. MW, molecular weight. GAPDH, glyceraldehyde-3-phosphate dehydrogenase.

cells. Notably, the iGePhos1 PhosTAC epimer showed moderate dephosphorylation at high concentration (1000 nM), possibly due to the EGFR inhibition effect of gefitinib itself. As a side-by-side control, we found that GePhos1 showed similar dephosphorylation potency beyond 100 nM when compared with gefitinib (Fig. 2A). The half-maximum dephosphorylation (DpC_{50}) for GePhos1 is around 13 nM in the engineered HeLa cells (fig. S9). In addition, after a high amount of EGF stimulation, we observed a reduction of total EGFR level, which was restored with the GePhos1 treatment (Fig. 2A). This is possibly due to the fact that GePhos1 blocked EGFR phosphorylation under strong EGF stimulation, which was known to induce EGFR phosphorylation followed by protein endocytosis and down-regulation (Fig. 2A) (*50*, *51*). In the absence of EGF stimulation, we did not observe substantial EGFR protein level change in DMSO, gefitinib, or GePhos1-treated FKBP12-PTPN2 HeLa cells after 24-hour incubation (fig. S10A). As a parallel control, the parental HeLa cells also showed high EGF-dependent EGFR phosphorylation and degradation. Those data suggest that the inverse correlation between EGFR phosphorylation and protein level is a conserved phenomenon and further supports the on-target mechanism of GePhos1 on EGFR (fig. S10B). To further confirm the phosphatase-dependent mechanism of GePhos1, a direct comparison of the impact when recruiting inactive or active PTPN2 phosphatase in the same cell line would be ideal. However, because of technical limitations in our system, we were only able to compare the inactive and active FKBP12-PTPN2 in separate stable cell lines. We generated a cell line expressing the inactive phosphatase mutant fused to FKBP12^{F36V}, named as FKBP12^{F36V}-PTPN2^{C216S}(TC45). In this FKBP12^{F36V}-PTPN2^{C216S}(TC45) cell line, we observed only slightly reduced EGFR phosphorylation with GePhos1 compared with iGePhos1 (Fig. 2C and fig. S11). Possible reasons for this minor phosphatase-independent effect may be the residual inhibition effect of gefitinib warhead, as well as that the GePhos1 recruitment of PTPN2 to EGFR sterically hinders *cis*- and/or *trans*-EGFR autophosphorylation in response to EGF stimulation.

Next, we tested EGFR phosphorylation and dephosphorylation kinetics upon treatment with EGF after pre-incubation with GePhos1 (Fig. 2B and fig. S7B). In the negative control iGePhos1-treated cells, EGFR pY1101, pY1068, and pY845 signals spiked around 2.5 min compared with no EGF stimulation at time 0 min and gradually decreased starting at 10 min after EGF stimulation, followed with phosphorylation of SHC (pY239/240), GRB2-associated binding protein 1 (GAB1) (pY627), mitogen-activated protein kinase kinase (MEK1/2) (pS217/221), extracellular signal-regulated protein kinases 1 and 2 (ERK1/2) (pT202/pY204), AKT (pS473), and STAT3 (pY705). In contrast, GePhos1 treatment substantially blunted EGFR phosphorylation at pY1101, pY1068, and pY845. Consistently, downstream signaling was also inhibited by GePhos1: we observed moderate increase of pSHC (pY239/240), faster turnover of pGAB1 (pY627) and pERK1/2 (pT202/Y204), delayed phosphorylation peak of MEK1/2 (pS217/221), and inhibited upregulation of pSTAT3 (pY705) (Fig. 2 and fig. S7). It is noteworthy that GePhos1 and iGePhos1 showed similar in vitro inhibitory effects toward EGFR [median inhibitory concentration (IC_{50}) = 0.38 and 0.29 nM, respectively; fig. S23), suggesting that the diminished inhibitory effect of iGePhos1 in the cellular assay was not a result of the modified FKBP12 ligand, which is in consistent with our proposed mechanism of PhosTAC.

Phosphoproteomic approach reveals altered EGFR signaling by PhosTAC

Next, a phosphoproteomic approach was used to investigate the phosphorylation changes associated with PhosTAC treatment (dataset S1). HeLa cells expressing FKBP12^{F36V}-PTPN2 were serum-starved while

treated with DMSO, GePhos1, iGePhos1, or gefitinib. All groups were then stimulated with EGF for 0 (no EGF), 7.5 or 15 min before sample collection. We chose 7.5 and 15 min due to the sample preparation bandwidth limitation and limited liquid chromatography–mass spectrometry testing throughput. Samples were digested and analyzed using a data-independent acquisition (DIA) proteomic approach (*52*). Proteomic data revealed the influence of GePhos1 on proteome-wide phosphorylation levels compared to iGePhos1. Using DIA-MS, we identified approximately 60,000 phospho-peptides in each sample (fig. S12). The number of substantially changed phosphopeptides detected in each treatment was visualized in the Venn plot (fig. S13A). In addition, a heatmap showed no substantial phosphorylation changes before EGF treatment (at 0 min) between DMSO-, gefitinib-, GePhos1-, or iGePhos1-treated groups (fig. S13B).

In agreement with previous data, dephosphorylation of the EGFR C-terminal tyrosine residues was validated via this independent and unbiased approach, including pY1068, pY1110, pY1172, and pY1197 (Fig. 3, A and B, and figs. S14 and 15A). In addition, GePhos1 robustly down-regulated multiple other phosphorylation sites of EGFR compared to DMSO and iGePhos1 (Fig. 3C and fig. S14A). Furthermore, we observed decreased phosphorylation of many downstream proteins such as SHC (pY426 and pY427), SOS1 (pS1333), ERK (pY187), and STAT3 (pY705) (figs. S14, B and C and S15), demonstrating PhosTAC's regulatory effect on EGFR signaling.

GePhos1 induced more significantly down-regulated protein phosphorylation when compared with iGePhos1 (Fig. 3D). Notably, we observed complex signaling consequences induced by GePhos1 (Fig. 3, D and E) with many phosphorylation sites being significantly altered in this study. For example, we observed significant dephosphorylation of EGFR pY1197, along with SHC pS426, inositol polyphosphate phosphatase-like 1 (INPPL1) [pY987 and pS1003; a regulator of EGFR (*53*, *54*)] (Fig. 3D), TK nonreceptor 2 (TNK2) (pY827) (*55*), and STAT3 (pY705) (Fig. 3E), showcasing the regulatory effect on EGFR signaling pathways through the PhosTAC

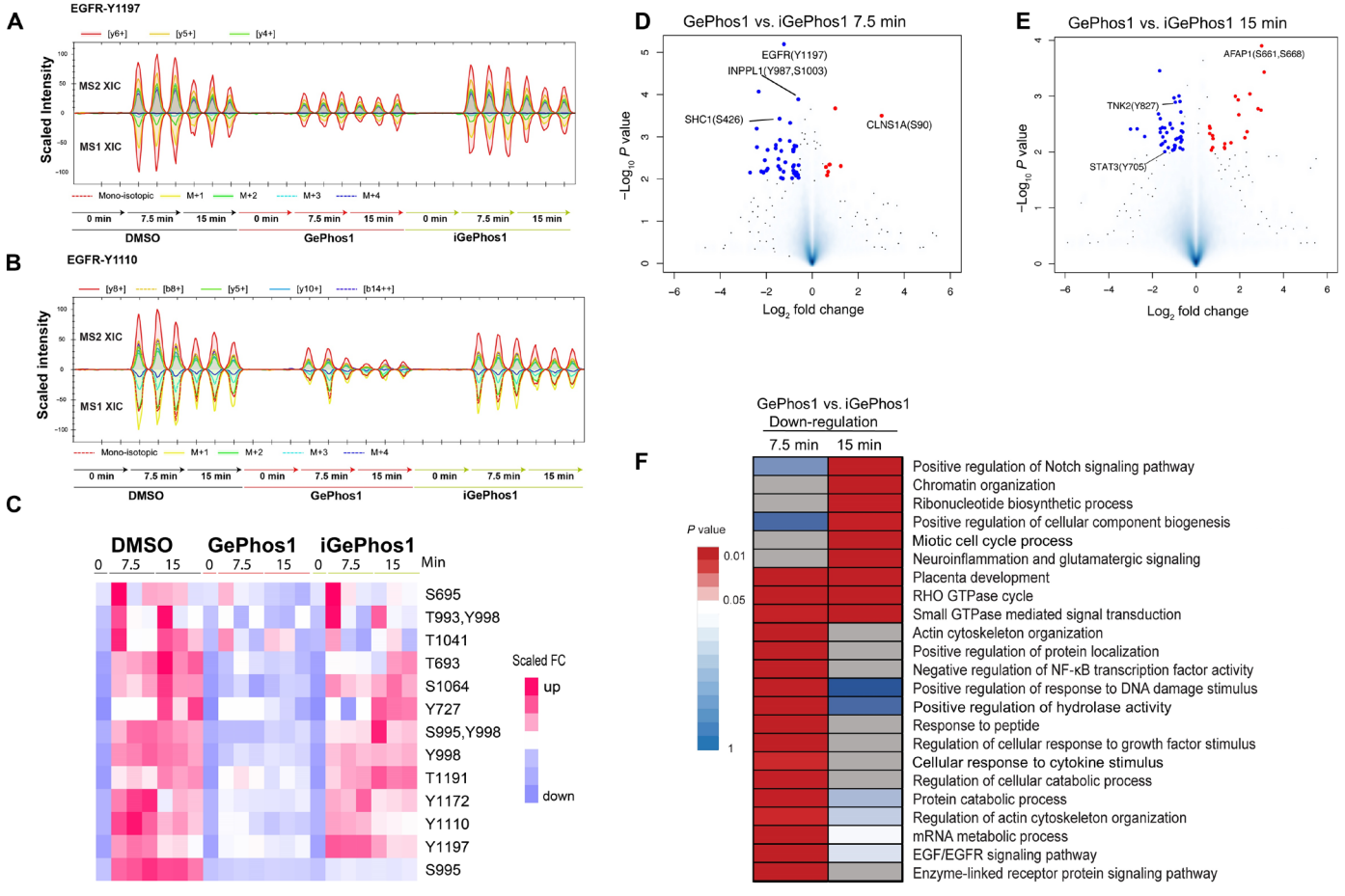

Fig. 3. GePhos1-induced dephosphorylation events confirmed by DIA-MS. (**A** and **B**) Extracted extracted ion chromatogram (XIC) graphs from Spectronaut software for EGFR phosphorylation sites pY1197 and pY1110. MS1 XIC indicates phosphopeptide data from the first mass spectrometer, and MS2 XIC indicates phosphopeptide data from the second mass spectrometer (MS/MS). Charges of peptides and fragments are indicated in the figure. (**C**) Heatmap for multiple significantly changed EGFR phosphorylation sites after PhosTAC treatment. Fold change was calculated by comparing to the average of 0 min control of each treatment respectively. (**D** and **E**) Volcano plot of DIA-MS proteomic profiling data comparing GePhos1 and iGePhos1 treatments. FKBP12^{F36V}-PTPN2 HeLa cells were treated with GePhos1 or iGePhos1 for 24 hours, followed by treatment with EGF (100 ng ml^{-1}) for 7.5 or 15 min. Fold change was calculated by comparing the peak intensity of GePhos1-treated phosphopeptides to iGePhos1-treated phospho-peptides. Blue dots indicate lower levels of phosphorylation in GePhos1 treatment compared to iGePhos1, and red dots indicate higher levels phosphorylation in GePhos1 treatment compared to iGePhos1. (**F**) GO functional annotation analysis of the enriched down-regulated phosphoproteins in GePhos1 treatment compared to iGePhos1 at 7.5 and 15 min. Three replicates were used for each condition. GTPase, guanosine triphosphatase. FC, fold change.

mechanism. A few protein phosphorylation levels were significantly increased in GePhos1-treated cells compared with iGePhos1, such as methylosome subunit pICIn [encoded by chloride nucleotide-sensitive channel 1A (*CLNS1A*)] pS90. However, the functional consequence and correlation with EGFR signaling remain to be elucidated (Fig. 3, D and E). We next enriched the top 100 proteins whose phosphorylation was significantly reduced by GePhos1 compared to iGePhso1 ($P < 0.05$) and applied these candidates to Gene Ontology (GO) analysis. It was shown that these dephosphorylated candidates are involved in pathways such as EGF/EGFR signaling, response to growth factor, and small and Ras homologous (RHO) GTPase–related signals, indicating the influence of GePhos1 on these pathways (Fig. 3F).

We next examined the different dephosphorylation patterns induced by gefitinib or GePhos1 because gefitinib functions through an occupancy-driven mechanism compared to GePhos1, which combined the occupancy- and event-driven mechanisms. After 7.5 min of EGF stimulation, gefitinib demonstrated stronger EGFR phosphorylation inhibition compared with GePhos1 in term of pY1197, while less obvious differences on other EGFR phosphorylation sites was observed. The comparatively less effects of GePhos1 to gefitinib on EGFR and downstream SHC (Y426 and Y427) (Fig. 4A) are attributable to its presumably poorer cell permeability due to its larger molecular size and less optimized structure as a proof-of-concept molecule. Notably, GePhos1 showed decreased inhibition toward receptor-interacting protein kinase 2 (S363) (Fig. 4A), a known off-target of gefitinib (*56*, *57*), suggesting a possible extra layer of target selectivity provided by the PhosTAC mechanism, which is also commonly found in PROTAC studies (*33*). We also observed GePhos1 treatment led to preferential eukaryotic translation initiation factor 4E binding protein 1 (EIF4EBP1) (pS85) dephosphorylation (*58*, *59*), whose function was associated with abnormal cell growth (*60*–*62*), indicating possible antiproliferative advantages of PhosTACs (Fig. 4A). After 15 min of EGF stimulation, more significant and distinct protein dephosphorylation events were observed between GePhos1- and gefitinib-treated groups (Fig. 4B). Notably, we observed preferential dephosphorylation of EIF4EBP1 (pS86), eukaryotic translation initiation factor 4B (pS406) (*63*, *64*), Capicua (pS77) (*65*), and yes-associated protein 1 (pT143) (*66*) by GePhos1, which again indicates possible inhibitory advantages compared to gefitinib (Fig. 4, A and B).

Next, we compared the top 100 proteins, whose phosphorylation events were significantly reduced by GePhos1 compared to gefitinib ($P < 0.05$). GO analysis revealed that these proteins are involved in EGF/EGFR signaling, Rho GTPase signaling, signaling by RTKs, etc., showcasing unique influence of GePhos1 on these pathways (Fig. 4C). We next explored the kinome and identified 116 kinases potentially affected in our phosphoproteomic study (Fig. 4D). When compared with gefitinib, GePhos1 preferentially affects the TK family, TK-like kinase family, and cyclin-dependent kinases (CDKs), glycogen synthase kinases, MAP kinases, and CDK-like kinases family (CGMC). In comparison with GePhos1, STE kinase family phosphorylation was preferentially down-regulated by gefitinib (Fig. 4E). The dynamic impacts on kinome phosphorylation by GePhos1 or gefitinib in the presence of EGF are visually represented via a heatmap, showcasing differential impacts of GePhos1. For example, phosphorylation of Unc-51–like kinase 1 (ULK1) (S330), P21 (RAC1)–activated kinase 4 (PAK4) (S181), MAPK1 (Y187), and AKT1(S122/124/126) were preferentially down-regulated by GePhos1 at 15 min compared with DMSO or gefitinib (Fig. 4F). Overall, these results indicate that GePhos1, via recruiting a phosphatase, affects phosphorylation through a different action than gefitinib, which directly inhibits EGFR kinase activity. This PhosTAC technology could provide an alternative avenue for RTK inhibition with possible selectivity and advantages. However, the phosphorylation signaling pathways modified by PhosTAC are of great complexity, and further investigation is required. Our PhosTACs enabled the biologically intriguing comparison of cell signaling consequences between the EGFR activity inhibition through drugs such as gefitinib and dual inhibitory mode of actions in GePhos1.

Covalent PhosTAC (AfaPhos1) induces EGFR dephosphorylation

One major challenge for clinical applications of EGFR TKIs is acquired drug resistance, e.g., mutations of EGFR at L858R/T790M lead to higher ATP affinity (*20*) or decreased TKI engagement, resulting in gefitinib resistance. One of the commonly used cell lines for mutated EGFR study is H1975, a non–small cell lung cancer cell line. To expand the PhosTAC application in cell lines harboring TKI-resistant mutations, we generated $FKBP12^{F36V}$-PTPN2–expressing H1975 cells. As expected, in H1975, L858R/T790M EGFR is constitutively phosphorylated under normal conditions, and EGF stimulation only slightly enhanced phosphorylation (fig. S16), which is of substantial contrast as observed in WT EGFR of HeLa (Fig. 2). In addition, GePhos1 or gefitinib treatment only demonstrated limited EGFR dephosphorylation (fig. S16) in H1975 irrespective of EGF stimulation. This is probably due to the limited engagement of the gefitinib molecule to mutated EGFR. To overcome the acquired TKI resistance, the next generation of TKIs, such as afatinib, containing cysteine reactive groups was developed to react with EGFR C797 and covalently bind to EGFR. When comparing the potency of gefitinib with afatinib in H1975, only afatinib effectively reduced EGFR phosphorylation under normal culture conditions (fig. S17). To effectively target mutated EGFR with PhosTAC, we designed a new EGFR PhosTAC based on afatinib as a warhead, named AfaPhos1 (Fig. 5A, left). Similar to iGePhos1, we synthesized inactive PhosTAC epimer with the $FKBP12^{F36V}$ epimer ligand (named iAfaPhos1; Fig 5A, right). As expected, we observed dose-dependent EGFR dephosphorylation at both pY1068 and pY845 with AfaPhos1 treatment, achieving 90% dephosphorylation at 0.5 μM [Fig. 5, B (left) and C, and fig. S18], while iAfaPhos1 displayed a blunted dose-dependent dephosphorylation effect, showing 90% dephosphorylation when dosing above 5 μM [Fig. 5, B (right) and C, and fig. S18]. The reduced inhibition efficiency disparity between AfaPhos1 and iAfaPhos1 compared to GePhos1 and iGePhos1 in HeLa is possibly due to the high potency of the afatinib warhead and loss of catalytic activity of covalent PhosTAC, which is also commonly observed for covalent PROTACs (*32*). We also observed notable dephosphorylation after 6-hour treatment of AfaPhos1 and GePhos1 (fig. S19); this is in accordance with the fast kinetic of phosphatase action and our tau PhosTAC study (*35*).

It is worth noting that due to the L858R/T790M mutations, H1975 EGFR has high phosphorylation level even without the EGF stimulation; thus, no EGF stimulation was applied in this experiment, and subsequently, no EGF-dependent total EGFR down-regulation was observed. Overall, our result demonstrates that the covalent ligands can be applied as potent warheads for future PhosTAC design.

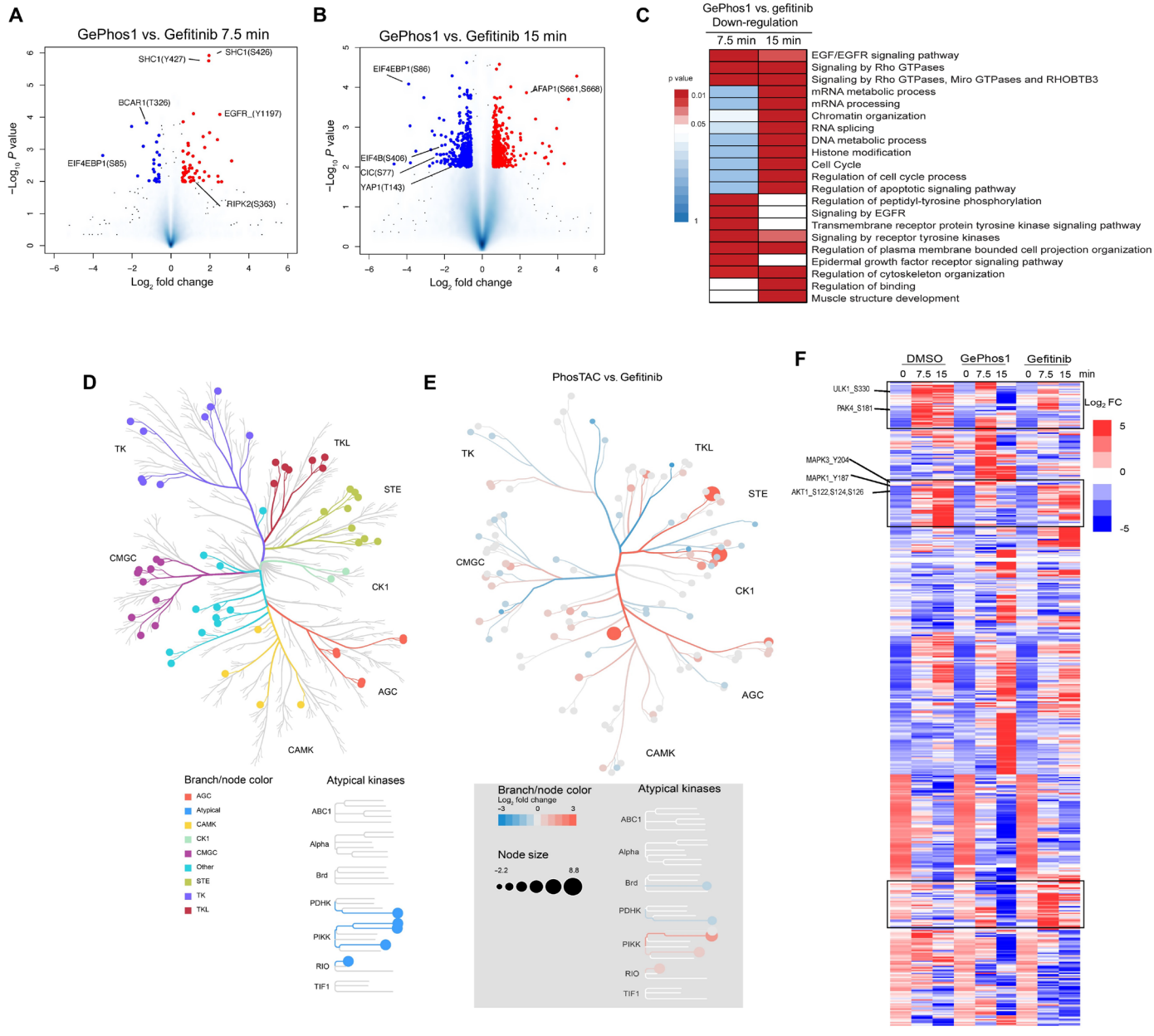

Fig. 4. GePhos1 induced proteome-wide dephosphorylation in a different patten compared to gefitinib. (**A** and **B**) Volcano plot of DIA-MS proteomic profiling data comparing GePhos1 and gefitinib treatments. $FKBP12^{F36V}$-PTPN2 HeLa cells treated with GePhos1 or gefitinib for 24 hours, followed by treatment with EGF (100 ng ml^{-1}) for 7.5 or 15 min. Fold change was calculated by comparing peak intensity of GePhos1-treated phospho-peptides to gefitinib-treated phospho-peptides. Blue dots indicate lower levels of decreased phosphorylation in GePhos1 treatment compared to gefitinib, red dots indicate higher levels of phosphorylation in GePhos1 treatment compared to gefitinib. (**C**) Selected pathways of GO analysis for enriched down-regulated phosphoproteins in GePhos1 treatment compared to gefitinib. (**D**) Phylogenetic tree of all protein kinases families detected in proteomic study. (**E**) Phylogenetic tree of protein kinases families affected by GePhos1 compared to gefitinib after 7.5 min of EGF stimulation. Fold change was calculated by comparing peak intensity of GePhos1-treated phospho-peptides to gefitinib-treated phospho-peptides. Blue dots indicate lower levels of phosphorylation in GePhos1 treatment compared to gefitinib, and red dots indicate higher levels of phosphorylation in GePhos1 treatment compared to gefitinib. TK, tyrosine kinase family; TKL, tyrosine kinase like kinase family; STE, serine/threonine kinase family; CK1, casein kinase 1 family; CAMK–Ca2+/calmodulin-dependent protein kinase family; CGMC, CDKs, glycogen synthase kinases (GSKs), MAP kinases and CDK-like kinases family. (**F**) Heatmap of all quantified kinase phosphorylation sites with indicated treatments. The fold change is calculated by comparing to the average of 0-min samples of each treatment, respectively. Several representative groups are framed in boxes, and EGFR signaling–related examples are labeled. Three replicates were used for each condition.

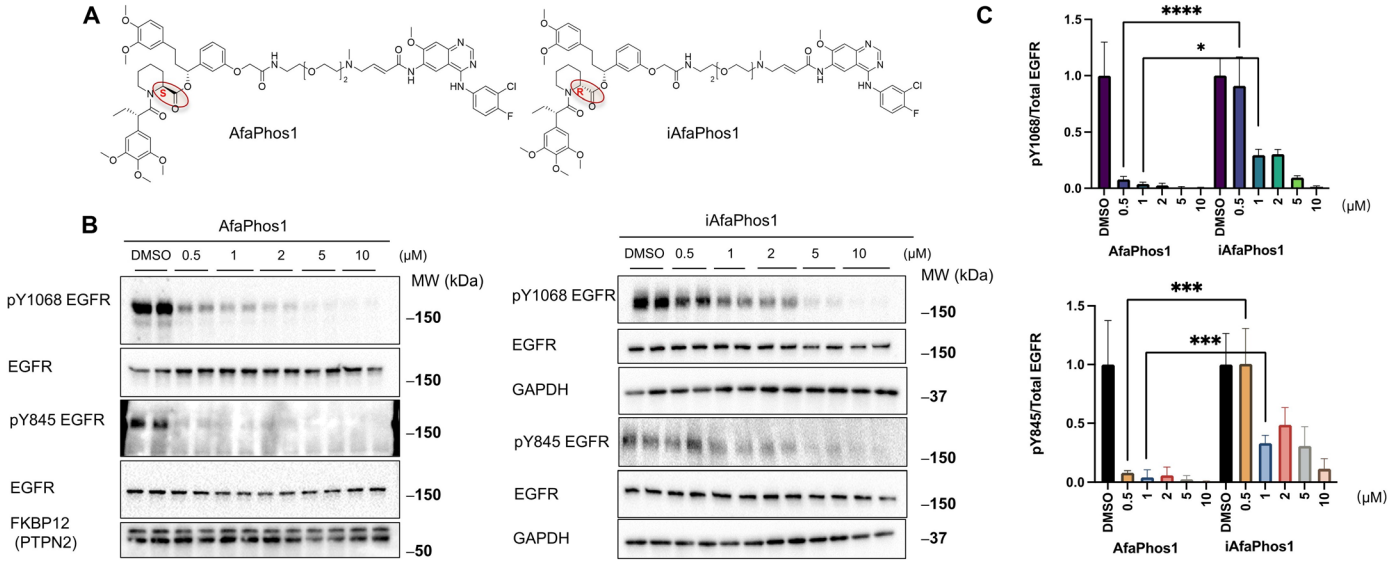

Fig. 5. Dephosphorylation of EGFR by afatinib-based PhosTAC (AfaPhos1) in EGFR mutant cells. (**A**) Structures of AfaPhos1 and iAfaPhos1. (**B**) AfaPhos1 induced significant dephosphorylation compared with iAfaPhos1. FKBP12^{F36V}-PTPN2 H1975 cells were treated with indicated concentrations of AfaPhos1 and iAfaPhos1 in full medium for 24 hours. Cell lysates were collected and analyzed by Western blot using indicated antibodies. (**C**) Quantification of phosphorylation level for Y1068 and Y846 of EGFR. Data were quantified from the phosphorylated or total EGFR proteins with five replicates and summarized as mean and SD. Significance was calculated with *t* test. Representative data of five replicates. *$P < 0.05$, ***$P < 0.001$, and ****$P < 0.0001$.

EGFR PhosTACs induce apoptosis and cell toxicity

EGFR signaling is critical for cell survival and proliferation; thus, we set to test the biological effect of EGFR PhosTACs. We tested the apoptosis-inducing effect of PhosTAC using annexin V and propidium iodide staining. After incubating cells with PhosTACs for 48 hours, we observed that GePhos1 and AfaPhos1 induced apoptosis and cell death in HeLa (Fig. 6A) and H1975 cells, respectively (Fig. 6B). Using CellTiter-Glo assay, which monitors the cellular ATP content, to measure cell viability, we observed that after 4 days of treatments, 5 μM GePhos1 resulted in a 48.5% decrease in cell viability, while the epimer displayed 20.6% decrease in FKBP12^{F36V}-PTPN2 HeLa cells. After 6 days of treatment, GePhos1 and gefitinib did not reach full inhibition of HeLa cells at 5 μM concentration, GePhos1 exhibited 78.5% (IC_{50} = 0.81 μM), epimer 23.4%, and gefitinib 74.3% (IC_{50} = 2.54 μM) (Fig. 6C and fig. S20B) cell viability inhibition in FKBP12^{F36V}-PTPN2 HeLa cells. In FKBP12^{F36V}-PTPN2 H1975 cells, we found that AfaPhos1 (5 μM) inhibited cell viability by 94.1%, while epimer decreased cell viability by 65.2% after 4 days of treatments. After 6 days, AfaPhos1 exhibited a 99.6% decrease in cell viability (IC_{50} = 1.26 μM), iAfaPhos1 a 57.6% decrease (IC_{50} = 2.58 μM), and afatinib (IC_{50} = 2.11 μM) (Fig. 6D and fig. S20D). Similar to the aforementioned, the inhibitory effect of iAfaPhos1 at high concentration is possible due to the high potency of the afatinib warhead, loss of catalytic activity of covalent PhosTAC, and H1975's dependence on EGFR. PhosTAC showed lower inhibition effect compared to TKIs in parental cell lines (fig. S20). Notably, GePhos1 can inhibit H1975 cell viability after 4 days of treatment when compared with iGePhos1 (fig. S21). These results together demonstrate the inhibitory effects of PhosTAC on cellular proliferation.

DISCUSSION

In conclusion, targeted protein dephosphorylation (TPDephos) represents a modality with potential for selective and effective protein regulation. TPDephos is relatively new but is growing rapidly: our laboratory reported PhosTACs for PDCD4, FOX3a (*34*), and tau (*35*); in addition, Zheng *et al.* (*36*), Yamazone *et al.* (*37*), Zhang *et al.* (*38*), and Simpson *et al.* (*67*) reported dephosphorylation of tau, AKT, ASK1, family with sequence similarity 83 member D, and ULK1, respectively. These studies represent exploratory and pioneering works in TPDephos, demonstrating the potential for basic and therapeutic research.

TPDephos with PhosTACs provides another therapeutic modality in addition to kinase inhibitors and degraders. With its unique event-driven mechanism, PhosTACs have the potential for more precise and potent inhibition of POI compared with kinase inhibitors. Targeted protein degradation with PROTACs (*68*), lysosome-targeting chimeras (*69*), and antibody-based PROTACs (*70*) have demonstrated great therapeutic value in recent years via removal of the POIs. Because many kinases have kinase-independent functions (*71*, *72*), the removal of the whole protein gives rise to the possibility of unexpected side effects. On the other hand, PhosTACs modulate POI phosphorylation levels without degrading the whole POI, so PhosTACs are expected to modulate POI with more precision, with more predictable outcomes.

In this PhosTAC model, we combined the inhibitory effect of a TKI and active dephosphorylation induced by a tyrosine phosphatase to achieve dual inhibition of EGFR. Notably, our work represents an example of harnessing a tyrosine-protein phosphatase (PTPN2) for RTK-targeted dephosphorylation by a small bifunctional molecule other than protein dimerizers (*73*), providing a modality for RTK inhibition, whose dysregulation has been

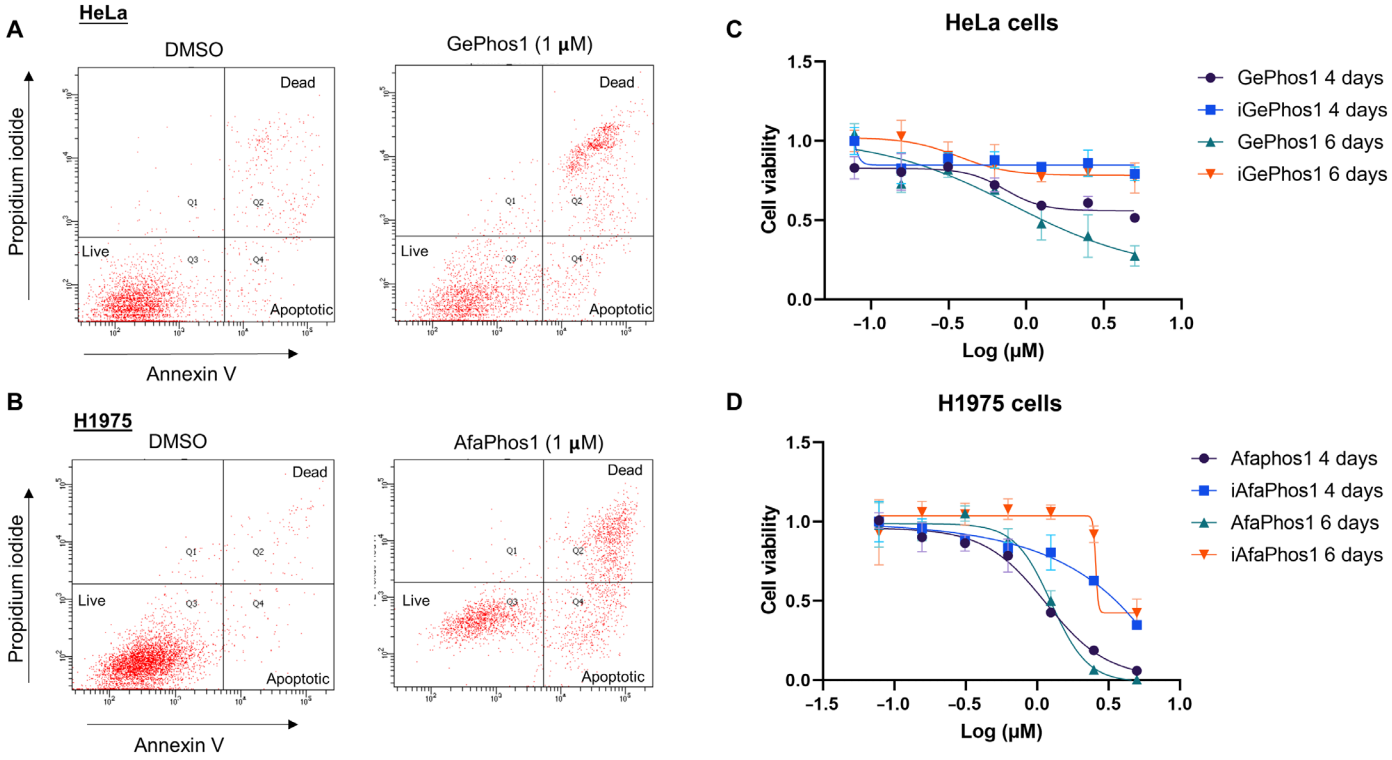

Fig. 6. GePhos1 and AfaPhos1 induce cancer cell apoptosis and toxicity. (**A** and **B**) Cell apoptosis assessed with propidium iodide–and annexin V-positive (PI^+/annexin V^+) by flow cytometry after treating HeLa cells and H1975 cells with GePhos1 (1 μM) or AfaPhos1 (1 μM), respectively, for 48 hours. GePhos1 resulted in 36.4% apoptotic and dead cells, and Afaphos1 resulted in 42.9% compared to 12.4 and 3.5% in DMSO-treated HeLa and H1975 cells, respectively. Shown are representative fluorescence-activated cell sorting data from two replicates. (**C** and **D**) HeLa cell (C) and H1975 cells (D) proliferation inhibited by PhosTACs. HeLa cells (C) and H1975 (D) cells are treated with indicated concentrations of GePhos1, iGePhos1, AfaPhos1, iAfaPhos1, respectively, for 4 or 6 days. Cell viabilities were tested using CellTiter-Glo, and data were quantified from three replicates and summarized as mean and SD. Data was normalized to DMSO-treated controls.

implicated in many types of diseases. Similarly, but on the flip side, the recent development of the phosphorylation-inducing chimeric small molecules (PHICS) platform for induced tyrosine phosphorylation certainly highlighted the importance and general interests in manipulating tyrosine phosphorylation (*74*). Also, we use phosphoproteomic method to study the signaling transductions affected by PhosTAC or similar concepts at the proteome-wide level. More intriguingly, the differential signaling pathways inhibited by PhosTAC compared with kinase inhibitor (gefitinib) suggest a potential window to manipulate related biological outcomes. It is also worth noting that we have designed an epimer control compound for the $FKBP^{F36V}$ protein, which provides a valuable tool compound, as the $FKBP12^{F36V}$ protein/degradation tag (dTAG) system is widely used in chemical biology studies. We subsequently designed a covalent afatinib-based PhosTAC to target the gatekeeper-mutated EGFR (L858R/T790M) and demonstrated its ability to dephosphorylate mutant EGFR. Consistent with predicted PhosTAC functions, EGFR PhosTACs induced apoptosis and inhibited cell viability in two different cancer cell lines.

As a category of bifunctional molecules, the development of PhosTACs still faces many challenges. For example, the current EGFR PhosTACs induced less pronounced dephosphorylation on EGFR (Fig. 4A) and downstream proteins when compared to TKIs such as gefitinib, which is attributable to their lower potency due to unoptimized structures, and presumably lower cell permeability due to the larger molecular sizes of these proof-of-concept PhosTACs. In addition, AfaPhos1, the covalent PhosTAC based on afatinib, demonstrated a lower efficacy disparity compared to the control, which is possibly due to the fact that its covalent nature prevents the "event-driven modality" of PhosTAC, indicating the limitation of covalent bifunctional molecules. Also, the PhosTAC induced downstream signaling pathways are exceptionally complex and need future investigations. In addition, no phosphatase activators have been well-established thus far, and the discovery of phosphatase ligands has been proven to be difficult.

However, with putatively >100 protein tyrosine phosphatases in the human genome and >30 protein Ser/Thr phosphatases along with their regulatory subunits, the possibility for future development of more efficient or target-specific PhosTACs is intriguing. The rapid dephosphorylation kinetics of phosphatases also may enable PhosTACs to modulate signaling quickly and effectively. In addition, the unique event-driven mechanism of bifunctional molecules may also provide PhosTACs with advantages such as selectivity and long-lasting effects. Overall, we demonstrated the feasibility of co-opting a TKI and a tyrosine phosphatase for PhosTACs, showcased their potential for targeted RTK dephosphorylation, and provided a dual inhibitory modality for both basic and translational research.

MATERIALS AND METHODS

Materials and instruments

Detailed information about materials and instruments is contained in the Supplementary Materials. All chemicals, reagents, and antibodies are used without modification unless specified.

Cell line, DNA constructs, and chemicals

Hela FlpIn-Trex (Thermo Fisher Scientific), HeLa derivative, and 293T cell lines were maintained and cultured with Dulbecco's modified Eagle's medium supplied with 10% fetal bovine serum (FBS) and 1% penicillin/streptomycin (P/S). H1975 lung cancer cell line (American Type Culture Collection) and its derivative were maintained in RPMI medium supplied with 10% FBS, 1% P/S, and additional glucose (4.5 g liter^{-1} final). All cell lines were incubated at 37°C with 5% CO_2. PTPN2_TC45 short isoform WT cDNA was inserted into *pcDNA5-FRT/TO-Flag-FKBP12^{F36V}* vector [modified from *pcDNA5-FRT/TO-Flag-FKBP12^{F36V}-PP2A A* in our previous report (*34*)] by Gibson assembly (E2611, NEB) to generate *pcDNA5-FRT/TO-Flag-FKBP12^{F36V}-PTPN2_TC45*. The phosphatase dead PTPN2^{C216S} was generated by site-directed mutagenesis (QuickChange II, Agilent) using the following primer pairs (5′-CCTGCGGTGATCCACAGTAGT GCAGGCATTGG-3′ and 5′-CCAATGCCTGCACTACTGTGGATC ACCGCAGG-3′) based on the PTPN2 WT sequence. The DNA sequence of *Flag-FKBP12^{F36V}-PTPN2* was amplified by polymerase chain reaction and assembled to pReceiver vector by Gibson assembly to generate a lentiviral vector carrying *Flag-FKBP12^{F36V}-PTPN2*. This *PTPN2* carrying vector was cotransfected with psPAX2 and pMD2.G into 293T cells by Trans-LT1 (Mirus Bio) to generate lentiviral particles, which were then used to transduce H1975 to establish a Flag-FKBP12^{F36V}-PTPN2–expressing cell line. EGF (R&D Systems) was reconstituted in sterile PBS and aliquoted for storage at −20°C.

FKBP12^{F36V} recombinant protein purification

pET15b-6XHis-FKBP12^{F36V} was purchased from Addgene (#73180). PTPN2 was cloned from *pcDNA5-FRT/TO-Flag-FKBP12^{F36V}-PTPN2* and assembled into *pET15b-6xHis-FKBP12^{F36V}* to generate *pET15b-6xHis-FKBP12^{F36V}-PTPN2* by Gibson assembly. To generate 6xHis-FKBP12^{F36V} recombinant proteins, either expression vector was first transformed into *Escherichia coli* BL21 (DE3) and cultured in a 2-liter Luria-Bertani flask. When optical density (OD_{600}) reached 0.6, 2 mM isopropyl β-D-thiogalactopyranoside was added for another 21.5-hour shaking at 18°C. After induction, the bacterium was collected and lysed in lysis buffer [50 mM Trizma HCl, 300 mM NaCl, 10 mM imidazole, 0.5 mM TCEP (pH 7.5), and protease inhibitor cocktail] followed by triple 3-min sonication (Branson Sonifier 450, 50% duty cycle, output control: 6) and centrifugation at 12,000 rpm for 20 min. The supernatant was then collected and inoculated in the nickel-nitrilotriacetic acid (Ni-NTA) resin. After washing and elution, the eluent was dialyzed against PBS with 4% glycerol overnight at 4°C. The dialyzed samples were briefly spun down to remove precipitated proteins, the clear supernatant was subjected to ITC (FKBP12^{F36V} protein) or size exclusion chromatography using S75 column (AKTA, GE Healthcare) (for FKBP12^{F36V} in SPR assay and FKBP12^{F36V}-PTPN2). The S75 column was equilibrated with PBS, and soluble protein fractions were aliquoted, snap-freezed, and stored at −80°C.

In vitro dephosphorylation

EGFR recombinant protein with kinase domain was purchased (Sino Biological, catalog no. 10001-H20B2) for in vitro dephosphorylation. For the in vitro dephosphorylation assay, the 6xHis-FKBP12^{F36V}-PTPN2 protein was dialyzed in reaction buffer [20 mM tris, 300 mM NaCl, 0.02% Triton X-100, 2 mM DTT, and 2 mM $MnCl_2$ (pH 7.5)]. A 5 μl of EGFR (160 nM) and 5 μl of 6xHis-FKBP12^{F36V}-PTPN2 (80 nM) are added to 84 μl of reaction buffer along with 5 μl of ATP solution (1 mM; Thermo Fisher Scientific, catalog no. R0441) in a clear 96-well plate. GePhos1 (1 μl, 400 nM), inactive GePhos1 (1 μl, 4 nM), or DMSO (1 μL) was added accordingly. The plate was then incubated at 37°C for 1 hour, and phosphate release was monitored by Malachite Green assay according to the manufacturer's protocol (Enzo Life Sciences, catalog no.BML-AK111-0250). Released phosphate concentrations were calculated from the standard curve generated with the phosphate standard solution.

SPR and ITC

All SPR experiments were performed on a Biacore 8K (Cytiva) at 25°C, and PBS-P+ (Cytiva) with 2% DMSO was used as the running buffer. 6xHis-FKBP12F36V was diluted in 10 mM sodium acetate (pH 5.5) and immobilized on a CM5 (Cytiva) chip using 1-ethyl-3-(3-dimethylaminopropyl)carbodiimide/*N*-hydroxysuccinimide coupling conditions until an immobilized resonance units (RU) of 3000 was achieved. For single-cycle experiments, a contact time of 120 s and dissociation time of 600 s was performed (30 μl/min), and both molecules were tested with a four-fold dilution series from 0.29–300 nM. For the multi-cycle experiment, a contact time of 120 s and dissociation time of 400 s were performed for each analyte concentration (40 μl/min). The active ligand was tested from 1.17 to 75 nM, while the epimer was tested from 3.9 to 1000 nM. After blank subtraction, reference subtraction, and solvent correction were applied, the kinetic model of 1:1 binding in Biacore Evaluation Software (Cytiva) was used to quantify binding. ITC experiments were done in a buffer composed of 137 mM NaCl, 2.7 mM KCl, 10 mM Na2HPO4, 1.8 mM KH2PO4, and 1% DMSO at 298 K using an Affinity ITC (TA instruments). The stirring speed is 125 rpm, the injection rate is 0.5 μl/s, and the cell volume is 182 μl. Baseline subtraction was performed using Blank (Constant) model subtraction in NanoAnalyze (TA Instruments). The titration sequence included 22 injections, 2.5 μl each, with a spacing of 180 s between the injections. The titration conditions were as follows: 110 μM FKBP12^{F36V} ligand or epimer ligand into 20 μM FKBP12^{F36V}. NanoAnalyze software (TA instruments) was used to analyze the raw ITC data.

Sample process, Western blotting, and antibodies

To analyze EGFR phosphorylation status, HeLa cells expressing FKBP12^{F36V}-PTPN2 were seeded into 12-well plates and serum-starved for 24 hours in the presence of DMSO or PhosTACs (as indicated in each experiment). EGF (final 100 ng ml^{-1}) was added for the last 15 min (or as indicated for each time point) of the incubation period before sample collection by radioimmunoprecipitation assay buffer with 1% SDS. The collected samples were then passed through a 22-gauge syringe 10 times to help lysing cells. The protein samples were quantified by bicinchoninic acid (BCA) assay, mixed with 4× sample buffer, boiled at 95°C for 5 min, and subjected to SDS–polyacrylamide gel electrophoresis using indicated antibodies. The antibodies used in this study as follows: anti-EGFR (Thermo Fisher Scientific, #MA5-13269), anti-EGFR pY1068 (Cell Signaling Technology, #3777), anti-EGFR pY1101 (Abcam, #ab76195), anti-EGFR pY845 (Cell Signaling Technology, #2231), anti-AKT (Cell Signaling Technology, #9272), anti-AKT pS473 (Cell Signaling Technology,

#4060 s), anti-ERK1/2 (Cell Signaling Technology, #4695), anti-ERK1/2 pT202/pY204 (Cell Signaling Technology, #4370), anti-STAT3 (Cell Signaling Technology, #4904), anti-STAT3 pY705 (Cell Signaling Technology, #9145), anti-SHC pY239/240 (Cell Signaling Technology, #2434), anti-GAB1 (Cell Signaling Technology, #3232), anti-GAB1 pY627 (Cell Signaling Technology, #3233P), anti-FKBP12 (Santa Cruz Biotechnology, #133067), anti–glyceraldehyde-3-phosphate dehydrogenase (Millipore, #MAB374), and anti-vinculin (Cell Signaling Technology, #13901). Quantification of Western blots was performed with Image Lab 6.1 software (Bio-Rad) following the manufacturer's instruction, and figures were created with Prism 9.0 or 10.

Ternary complex pull-down assay

FKBP12^{F36V}-PTPN2–expressing HeLa cells were serum-starved and treated with dimethyl sulfoxide (DMSO), GePhos1 (1000 nM), or iGePhos1 (1000 nM) for 24 hours. The cells were then collected with lysis buffer (150 mM NaCl, 1 mM EDTA, 25 mM tris-HCl, and 1% Triton X-100) and centrifuged at 15,000 rpm for 20 min at 4°C to collect the supernatant. After BCA analysis, 1 mg of each supernatant (adjusted to total volume 500 μl) was co-incubated and rotated with anti-FKBP12 antibody (20 μl; Santa Cruz Biotechnology, H-5, #SC-133067) for 16 hours at 4°C. The agarose beads (40-μl beads slurry; Millipore, protein G agarose, #16-266) were then added to each lysate for an additional 8 hours to immuno-precipitate FKBP12^{F36V}-PTPN2–associated proteins. The agarose beads were then washed with 1 ml of lysis buffer for three times, eluted with sample buffer, and analyzed via Western blotting using indicated antibodies. Anti-PTPN2 antibody (ABclonal, #A1808) and anti-EGFR (Thermo Fisher Scientific, #MA5-13269).

In vitro HTRF KinEASE assay

ATP & Substrate solution (2×) and kinase solution (2×) were prepared using assay buffer (HTRF KinEASE TK kit, PerkinElmer, 62TK0PEJ). A 50 nl of compound was transferred to 384 assay plate (Greiner, 784075). The added 2.5 μl of 2× kinase solution was mixed and incubated in a polystyrene-coated 384 assay plate for 10 min at 25°C. A 2.5 μl of 2× Substrate & ATP solution was added to the well and incubated at 25°C for 60 min. XL665 & Antibody solution (2×) were prepared with detection buffer. A 5 μl of kinase detection reagent was added to the well and incubated for 60 min at 25°C. The fluorescence signals of 620 nm (Cryptate) and 665 nm (XL665) were read by microtiter-plate reader (BMG, PHERAstar FSX).

Cell culture for phosphoproteomics

HeLa cells expressing FKBP12^{F36V}-PTPN2 were seeded into 10-cm culture dishes until 80% confluency. All dishes were then washed with PBS once and treated with serum-free medium together with DMSO, GePhos1 (500 nM), inactive GePhos1 (500 nM), or gefitinib (500 nM) (three replicates for each group) for 24 hours. At the last 15 min, cells were then treated with EGF (final 100 ng ml^{-1}) for 7.5 or 15 min. No EGF treatment was applied for 0-min sample. To collect samples for mass spectrometry, all medium were removed, rinsed with cold PBS once, and immediately snap-frozen by liquid nitrogen. All cells were then scraped down by cell scrapers using 500 μl of 10 M urea containing cOmplete protease inhibitor cocktail (Roche, #11697498001) and PhoSTOP phosphatase inhibitor cocktail (Roche, #4906845001), snap-frozen in liquid nitrogen, and store at −80°C until sample processing. Three replicates were used for each condition.

Sample preparation for phosphoproteomics

As described in the previous study (*52*), the cell samples were lysed by sonication at 4°C for two cycles (1 min per cycle) using a VialTweeter device (Hielscher-Ultrasound Technology) (*75*, *76*) and then centrifuged at 20,000*g* for 1 hour to remove the insoluble material. The protein concentration assay was performed using the Bio-Rad protein assay dye, and a total of 700 μg of protein mixture was transferred to new 2-ml Eppendorf tubes for alkylation reduction reaction. The protein mixture was reduced with a final concentration of 10 mM tris-(2-carboxyethyl)-phosphine and incubated for 1 hour at 37°C. The following alkylation was performed with 20 mM iodoacetamide in the dark for 1 hour at room temperature. After the reduction, for trypsin digestion, all the samples were diluted five times with the 100 mM NH_4HCO_3 and digested with sequencing grade porcine trypsin (Promega) at a ratio of 1:20 overnight at 37°C. The peptide mixture was purified with a C18 column (MacroSpin Columns, NEST Group INC). The amount of the final peptides was determined by NanoDrop (Thermo Fisher Scientific).

For the phosphopeptide enrichment, 250 μg of purified peptide mixture was processed using the High-Select Fe-NTA kit (Thermo Fisher Scientific, #A32992). The enrichment protocol was the same as described previously (*77*). Briefly, the resins of one tube in the kit were used for five samples equally. The peptide-resin mixture was incubated for 30 min at room temperature and gently shaken for 10 min and then transferred into the filter tip (TF-20-L-R-S, Axygen) to remove the supernatant by centrifugation. Then, the resins binding phosphopeptides were washed sequentially with 200 μl × 3 washing buffer (80% ACN and 0.1% trifluoroacetic acid) and 200 μl × 3 H_2O to remove nonspecifically peptides. The phosphopeptides were eluted from the resins by 100 μl × 2 elution buffer (50% ACN and 5% NH_3•H_2O) and dried with SpeedVac (Thermo Fisher Scientific). All centrifugation steps above were conducted at 500*g* for 30 s. The eluates were dried immediately with SpeedVac and resuspended with buffer A for future MS analysis.

Data-independent acquisition mass spectrometry

The samples were measured by the DIA-MS method as described previously. (*78*–*80*) The Orbitrap Eclipse Tribrid mass spectrometer (Thermo Fisher Scientific) instrument coupled to the EASY-nLC 1200 systems (Thermo Fisher Scientific, San Jose, CA). For the data acquisition, the total 150-min gradient was used at the flow rate of 300 nl/min with the temperature controlled at 60°C using a column oven. The method consisted of one MS1 scan and 33 variable windowed MS2 scans [with 1 mass/charge ratio (*m*/*z*) overlapping between isolation windows]. The MS1 scan range was 350 to 1650 *m*/*z*, and the MS1 resolution was 120,000 at *m*/*z* 200. The MS1 full scan automatic gain control (AGC) target value was set to 500%, and the maximum injection time was 100 ms. The MS2 resolution was set to 30,000 at *m*/*z* 200 with the MS2 scan range 200 to 1800 *m*/*z*, and the normalized higher-energy collisional dissociation (HCD) collision energy was 28%. The MS2 AGC was set to 4000%, and the maximum injection time was 52 ms. The default peptide charge state was set to 2. Both MS1 and MS2 spectra were recorded in profile mode.

Data analysis

The Spectronaut v16 (*81*–*83*) was used for the DIA data analysis with the direct DIA algorithm. For the phosphorylation site collapse from different precursors based on two rules: (i) the less missing value was selected; (ii) for the multiple precursors that have the same number of

missing values, the highest intensity one was selected. The oxidation at methionine and the phosphorylation at S/T/Y were set as variable modifications, whereas carbamidomethylation at cysteine was set as fixed modification. To quantify phosphorylation sites across conditions, the probability of posttranslational modifications cutoff was set at 0.75 and 0 to report two datasets, for phosphosite localization and quantification, respectively. This means that for a specific phosphorylation site, the PTM score was above 0.75 for at least one sample to localize the phosphosites in the peptide, as we reported previously (*84*). Both peptide and protein false discovery rate cutoffs (*Q* value) were controlled below 1%. All the other Spectronaut settings are kept as default.

The plots were created by R packages ("ggplot" and" pheatmap"). Functional annotation analysis was performed on the online tool MetaScape with Expression Analysis function (https://metascape.org/gp/index.html#/main/step1).

Phosphoproteomics data availability

All the MS-based phosphor-DIA datasets have been deposited to the ProteomeXchange Consortium via the PRIDE partner repository (*85*) with the dataset identifier PXD038022.

Apoptosis and cell viability assay

For the analysis of apoptosis, HeLa and H1975 cells were seeded in six-well plates for 24 hours, after which, the medium was changed to serum-free medium. DMSO, GePhos1 (1 μM), or inactive GePhos1 was added to HeLa cells, while DMSO, AfaPhos1 (1 μM), or inactive AfaPhos1 was added to H1975 cells. Both HeLa cells and H1975 cells were treated for 48 hours before being collected. HeLa cells and H1975 cells were isolated and stained according to the manufacturer's protocol. Briefly, trypsinized cells were pelleted by centrifugation at 300*g* for 5 min, washed once with PBS, and resuspended in binding containing propidium iodide and annexin V Alexa Fluor 488 (Invitrogen, catalog no. V13241). Following a 15-min incubation, the cells were diluted with binding buffer to a final volume of 0.5 ml, and the fluorescence was detected with BD Biosciences LSRFortessa flow cytometer. Data were analyzed with BD FACSDiva Software.

For the cell viability assay, HeLa cells expressing $FKBP12^{F36V}$-PTPN2 were seeded as 3000 cells per well in 96-well plates (Corning, #3610) in full medium for 24 hours and then treated with GePhos1 or iGePhos1 in serum-free conditions for 4 or 6 days. H1975 cells expressing $FKBP12^{F36V}$-PTPN2 were seeded as 3000 cells per well in 96-well plates (Corning, #3610) in full medium for 24 hours and then treated with AfaPhos1 or iAfaPhos1 in serum-free conditions for 4 or 6 days. The relative cell viability was measured by CellTiter-Glo (Promega, catalog no.G9241) with a plate reader (Tecan Spark) following the manufacturer's protocol and normalized against DMSO control for each treatment. Data presented are mean and SDs from three biology replicates. Data were processed with Prims 9.0.

Supplementary Materials

This PDF file includes:

Supplementary Text
Figs. S1 to S23

REFERENCES AND NOTES

1. P. Wee, Z. Wang, Epidermal growth factor receptor cell proliferation signaling pathways. *Cancers* **9**, 52 (2017).
2. H. Ogiso, R. Ishitani, O. Nureki, S. Fukai, M. Yamanaka, J.-H. Kim, K. Saito, A. Sakamoto, M. Inoue, M. Shirouzu, S. Yokoyama, Crystal structure of the complex of human epidermal growth factor and receptor extracellular domains. *Cell* **110**, 775–787 (2002).
3. A. Ullrich, L. Coussens, J. S. Hayflick, T. J. Dull, A. Gray, A. W. Tam, J. Lee, Y. Yarden, T. A. Libermann, J. Schlessinger, J. Downward, E. L. V. Mayes, N. Whittle, M. D. Waterfield, P. H. Seeburg, Human epidermal growth factor receptor cDNA sequence and aberrant expression of the amplified gene in A431 epidermoid carcinoma cells. *Nature* **309**, 418–42 (1984).
4. J. P. Dawson, M. B. Berger, C. C. Lin, J. Schlessinger, M. A. Lemmon, K. M. Ferguson, Epidermal growth factor receptor dimerization and activation require ligand-induced conformational changes in the dimer interface. *Mol. Cell. Biol.* **25**, 7734–7742 (2005).
5. X. Zhang, J. Gureasko, K. Shen, P. A. Cole, J. Kuriyan, An allosteric mechanism for activation of the kinase domain of epidermal growth factor receptor. *Cell* **125**, 1137–1149 (2006).
6. J. Schlessinger, M. A. Lemmon, SH2 and PTB domains in tyrosine kinase signaling. *Sci. STKE* **2003**, RE12 (2003).
7. M. F. Moran, C. A. Koch, D. Anderson, C. Ellis, L. England, G. S. Martin, T. Pawson, Src homology region 2 domains direct protein-protein interactions in signal transduction. *Proc. Natl. Acad. Sci. U.S.A.* **87**, 8622–8626 (1990).
8. A. G. Batzer, D. Rotin, J. M. Urena, E. Y. Skolnik, J. Schlessinger, Hierarchy of binding sites for Grb2 and Shc on the epidermal growth factor receptor. *Mol. Cell. Biol.* **14**, 5192–5201 (1994).
9. M. Ono, M. Kuwano, Molecular mechanisms of epidermal growth factor receptor (EGFR) activation and response to gefitinib and other EGFR-targeting drugs. *Clin. Cancer Res.* **12**, 7242–7251 (2006).
10. K. Sato, A. Sato, M. Aoto, Y. Fukami, c-Src phosphorylates epidermal growth factor receptor on tyrosine 845. *Biochem. Biophys. Res. Commun.* **215**, 1078–1087 (1995).
11. K. Sato, Cellular functions regulated by phosphorylation of EGFR on Tyr845. *Int. J. Mol. Sci.* **14**, 10761–10790 (2013).
12. D. A. Tice, J. S. Biscardi, A. L. Nickles, S. J. Parsons, Mechanism of biological synergy between cellular Src and epidermal growth factor receptor. *Proc. Natl. Acad. Sci. U.S.A.* **96**, 1415–1420 (1999).
13. S. Sigismund, D. Avanzato, L. Lanzetti, Emerging functions of the EGFR in cancer. *Mol. Oncol.* **12**, 3–20 (2018).
14. C. Braicu, M. Buse, C. Busuioc, R. Drula, D. Gulei, L. Raduly, A. Rusu, A. Irimie, A. G. Atanasov, O. Slaby, C. Ionescu, I. Berindan-Neagoe, A comprehensive review on MAPK: A promising therapeutic target in cancer. *Cancers* **11**, (2019).
15. H. Yu, D. Pardoll, R. Jove, STATs in cancer inflammation and immunity: A leading role for STAT3. *Nat. Rev. Cancer* **9**, 798–809 (2009).
16. M. Sibilia, R. Kroismayr, B. M. Lichtenberger, A. Natarajan, M. Hecking, M. Holcmann, The epidermal growth factor receptor: From development to tumorigenesis. *Differentiation* **75**, 770–787 (2007).
17. N. Normanno, A. De Luca, C. Bianco, L. Strizzi, M. Mancino, M. R. Maiello, A. Carotenuto, G. De Feo, F. Caponigro, D. S. Salomon, Epidermal growth factor receptor (EGFR) signaling in cancer. *Gene* **366**, 2–16 (2006).
18. N. Karachaliou, M. Fernandez-Bruno, J. W. P. Bracht, R. Rosell, EGFR first- and second-generation TKIs-there is still place for them in EGFR-mutant NSCLC patients. *Transl. Cancer Res.* **8**, S23–S47 (2019).
19. S. Kobayashi, T. J. Boggon, T. Dayaram, P. A. Janne, O. Kocher, M. Meyerson, B. E. Johnson, M. J. Eck, D. G. Tenen, B. Halmos, EGFRMutation and resistance of non-small-cell lung cancer to gefitinib. *N. Engl. J. Med.* **352**, 786–792 (2005).
20. C. H. Yun, K. E. Mengwasser, A. V. Toms, M. S. Woo, H. Greulich, K. K. Wong, M. Meyerson, M. J. Eck, The T790M mutation in EGFR kinase causes drug resistance by increasing the affinity for ATP. *Proc. Natl. Acad. Sci. U.S.A.* **105**, 2070–2075 (2008).
21. Z. Yang, N. Yang, Q. Ou, Y. Xiang, T. Jiang, X. Wu, H. Bao, X. Tong, X. Wang, Y. W. Shao, Y. Liu, Y. Wang, C. Zhou, Investigating novel resistance mechanisms to third-generation EGFR tyrosine kinase inhibitor osimertinib in non-small cell lung cancer patients. *Clin. Cancer Res.* **24**, 3097–3107 (2018).
22. H. B. Liu, Y. Wu, T. F. Lv, Y. W. Yao, Y. Y. Xiao, D. M. Yuan, Y. Song, Skin rash could predict the response to EGFR tyrosine kinase inhibitor and the prognosis for patients with non-small cell lung cancer: A systematic review and meta-analysis. *PLOS ONE* **8**, e55128 (2013).
23. L. C. Tseng, K. H. Chen, C. L. Wang, L. C. Weng, Effects of tyrosine kinase inhibitor therapy on skin toxicity and skin-related quality of life in patients with lung cancer: An observational study. *Medicine* **99**, e20510 (2020).
24. M. E. Lacouture, Mechanisms of cutaneous toxicities to EGFR inhibitors. *Nat. Rev. Cancer* **6**, 803–812 (2006).
25. I. Nasa, A. N. Kettenbach, Coordination of protein kinase and phosphoprotein phosphatase activities in mitosis. *Front. Cell Dev. Biol.* **6**, 30 (2018).
26. T. Tiganis, B. E. Kemp, N. K. Tonks, The protein-tyrosine phosphatase TCPTP regulates epidermal growth factor receptor-mediated and phosphatidylinositol 3-kinase-dependent signaling. *J. Biol. Chem.* **274**, 27768–27775 (1999).
27. T. Tiganis, A. M. Bennett, K. S. Ravichandran, N. K. Tonks, Epidermal growth factor receptor and the adaptor protein p52Shc are specific substrates of T-cell protein tyrosine phosphatase. *Mol. Cell. Biol.* **18**, 1622–1634 (1998).

28. M. Kohn, Turn and face the strange: A new view on phosphatases. *ACS Cent. Sci.* **6**, 467–477 (2020).
29. L. M. Scott, H. R. Lawrence, S. M. Sebti, N. J. Lawrence, J. Wu, Targeting protein tyrosine phosphatases for anticancer drug discovery. *Curr. Pharm. Des.* **16**, 1843–1862 (2010).
30. A. C. Lai, C. M. Crews, Induced protein degradation: An emerging drug discovery paradigm. *Nat. Rev. Drug Discov.* **16**, 101–114 (2017).
31. A. Testa, S. J. Hughes, X. Lucas, J. E. Wright, A. Ciulli, Structure-Based design of a macrocyclic PROTAC. *Angew. Chem. Int. Ed. Engl.* **59**, 1727–1734 (2020).
32. M. J. Bond, L. Chu, D. A. Nalawansha, K. Li, C. M. Crews, Targeted degradation of oncogenic KRAS(G12C) by VHL-recruiting PROTACs. *ACS Cent. Sci.* **6**, 1367–1375 (2020).
33. Z. Hu, C. M. Crews, Recent developments in PROTAC-mediated protein degradation: From bench to clinic. *Chembiochem* **23**, e202100270 (2022).
34. P. H. Chen, Z. Hu, E. An, I. Okeke, S. Zheng, X. Luo, A. Gong, S. Jaime-Figueroa, C. M. Crews, Modulation of phosphoprotein activity by phosphorylation targeting chimeras (PhosTACs). *ACS Chem. Biol.* **16**, 2808–2815 (2021).
35. Z. Hu, P. H. Chen, W. Li, T. Douglas, J. Hines, Y. Liu, C. M. Crews, Targeted dephosphorylation of tau by phosphorylation targeting chimeras (PhosTACs) as a therapeutic modality. *J. Am. Chem. Soc.* **145**, 4045–4055 (2023).
36. J. Zheng, N. Tian, F. Liu, Y. Zhang, J. Su, Y. Gao, M. Deng, L. Wei, J. Ye, H. Li, J. Z. Wang, A novel dephosphorylation targeting chimera selectively promoting tau removal in tauopathies. *Signal Transduct. Target. Ther.* **6**, 269 (2021).
37. S. Yamazoe, J. Tom, Y. Fu, W. Wu, L. Zeng, C. Sun, Q. Liu, J. Lin, K. Lin, W. J. Fairbrother, S. T. Staben, Heterobifunctional molecules induce dephosphorylation of kinases-a proof of concept study. *J. Med. Chem.* **63**, 2807–2813 (2020).
38. Q. Zhang, X. Wu, H. Zhang, Q. Wu, M. Fu, L. Hua, X. Zhu, Y. Guo, L. Zhang, Q. You, L. Wang, Protein phosphatase 5-recruiting chimeras for accelerating apoptosis-signal-regulated kinase 1 dephosphorylation with antiproliferative activity. *J. Am. Chem. Soc.* **145**, 1118–1128 (2023).
39. T. Clackson, W. Yang, L. W. Rozamus, M. Hatada, J. F. Amara, C. T. Rollins, L. F. Stevenson, S. R. Magari, S. A. Wood, N. L. Courage, X. Lu, F. Cerasoli Jr., M. Gilman, D. A. Holt, Redesigning an FKBP-ligand interface to generate chemical dimerizers with novel specificity. *Proc. Natl. Acad. Sci. U.S.A.* **95**, 10437–10442 (1998).
40. P. Ottis, M. Toure, P. M. Cromm, E. Ko, J. L. Gustafson, C. M. Crews, Assessing different E3 ligases for small molecule induced protein ubiquitination and degradation. *ACS Chem. Biol.* **12**, 2570–2578 (2017).
41. B. Nabet, F. M. Ferguson, B. K. A. Seong, M. Kuljanin, A. L. Leggett, M. L. Mohardt, A. Robichaud, A. S. Conway, D. L. Buckley, J. D. Mancias, J. E. Bradner, K. Stegmaier, N. S. Gray, Rapid and direct control of target protein levels with VHL-recruiting dTAG molecules. *Nat. Commun.* **11**, 4687 (2020).
42. J. Salami, S. Alabi, R. R. Willard, N. J. Vitale, J. Wang, H. Dong, M. Jin, D. P. McDonnell, A. P. Crew, T. K. Neklesa, C. M. Crews, Androgen receptor degradation by the proteolysis-targeting chimera ARCC-4 outperforms enzalutamide in cellular models of prostate cancer drug resistance. *Commun. Biol.* **1**, 100 (2018).
43. A. Testa, X. Lucas, G. V. Castro, K. H. Chan, J. E. Wright, A. C. Runcie, M. S. Gadd, W. T. A. Harrison, E. J. Ko, D. Fletcher, A. Ciulli, 3-Fluoro-4-hydroxyprolines: Synthesis, Conformational Analysis, and Stereoselective Recognition by the VHL E3 Ubiquitin Ligase for Targeted Protein Degradation. *J. Am. Chem. Soc.* **140**, 9299–9313 (2018).
44. S. W. Michnick, M. K. Rosen, T. J. Wandless, M. Karplus, S. L. Schreiber, Solution structure of FKBP, a rotamase enzyme and receptor for FK506 and rapamycin. *Science* **252**, 836–839 (1991).
45. D. A. Holt, J. I. Luengo, D. S. Yamashita, H. J. Oh, A. L. Konialian, H. K. Yen, L. W. Rozamus, M. Brandt, M. J. Bossard, M. A. Levy, D. S. Eggleston, J. Liang, L. W. Schultz, T. J. Stout, J. Clardy, Design, synthesis, and kinetic evaluation of high-affinity FKBP ligands and the X-ray crystal structures of their complexes with FKBP12. *J. Am. Chem. Soc.* **115**, 9925–9938 (1993).
46. B. Nabet, J. M. Roberts, D. L. Buckley, J. Paulk, S. Dastjerdi, A. Yang, A. L. Leggett, M. A. Erb, M. A. Lawlor, A. Souza, T. G. Scott, S. Vittori, J. A. Perry, J. Qi, G. E. Winter, K. K. Wong, N. S. Gray, J. E. Bradner, The dTAG system for immediate and target-specific protein degradation. *Nat. Chem. Biol.* **14**, 431–441 (2018).
47. K. M. Marks, P. D. Braun, G. P. Nolan, A general approach for chemical labeling and rapid, spatially controlled protein inactivation. *Proc. Natl. Acad. Sci. U.S.A.* **101**, 9982–9987 (2004).
48. D. P. Bondeson, A. Mares, I. E. Smith, E. Ko, S. Campos, A. H. Miah, K. E. Mulholland, N. Routly, D. L. Buckley, J. L. Gustafson, N. Zinn, P. Grandi, S. Shimamura, G. Bergamini, M. Faelth-Savitski, M. Bantscheff, C. Cox, D. A. Gordon, R. R. Willard, J. J. Flanagan, L. N. Casillas, B. J. Votta, W. den Besten, K. Famm, L. Kruidenier, P. S. Carter, J. D. Harling, I. Churcher, C. M. Crews, Catalytic in vivo protein knockdown by small-molecule PROTACs. *Nat. Chem. Biol.* **11**, 611–617 (2015).
49. J. P. Singh, Y. Li, Y. Y. Chen, S. D. Hsu, R. Page, W. Peti, T. C. Meng, The catalytic activity of TCPTP is auto-regulated by its intrinsically disordered tail and activated by Integrin alpha-1. *Nat. Commun.* **13**, 94 (2022).
50. Y. Zhou, H. Sakurai, New trend in ligand-induced EGFR trafficking: A dual-mode clathrin-mediated endocytosis model. *J. Proteomics* **255**, 104503 (2022).
51. S. Sigismund, V. Algisi, G. Nappo, A. Conte, R. Pascolutti, A. Cuomo, T. Bonaldi, E. Argenzio, L. G. Verhoef, E. Maspero, F. Bianchi, F. Capuani, A. Ciliberto, S. Polo, P. P. Di Fiore, Threshold-controlled ubiquitination of the EGFR directs receptor fate. *EMBO J.* **32**, 2140–2157 (2013).
52. B. Salovska, W. Li, Y. Di, Y. Liu, BoxCarmax: A high-selectivity data-independent acquisition mass spectrometry method for the analysis of protein turnover and complex samples. *Anal. Chem.* **93**, 3103–3111 (2021).
53. N. K. Prasad, S. J. Decker, SH2-containing 5′-inositol phosphatase, SHIP2, regulates cytoskeleton organization and ligand-dependent down-regulation of the epidermal growth factor receptor. *J. Biol. Chem.* **280**, 13129–13136 (2005).
54. N. K. Prasad, SHIP2 phosphoinositol phosphatase positively regulates EGFR-Akt pathway, CXCR4 expression, and cell migration in MDA-MB-231 breast cancer cells. *Int. J. Oncol.* **34**, 97–105 (2009).
55. K. Mahajan, N. P. Mahajan, ACK1/TNK2 tyrosine kinase: Molecular signaling and evolving role in cancers. *Oncogene* **34**, 4162–4167 (2015).
56. J. T. Tigno-Aranjuez, J. M. Asara, D. W. Abbott, Inhibition of RIP2's tyrosine kinase activity limits NOD2-driven cytokine responses. *Genes Dev.* **24**, 2666–2677 (2010).
57. N. Verma, A. K. Rai, V. Kaushik, D. Brunnert, K. R. Chahar, J. Pandey, P. Goyal, Identification of gefitinib off-targets using a structure-based systems biology approach; their validation with reverse docking and retrospective data mining. *Sci. Rep.* **6**, 33949 (2016).
58. A. C. Gingras, B. Raught, S. P. Gygi, A. Niedzwiecka, M. Miron, S. K. Burley, R. D. Polakiewicz, A. Wyslouch-Cieszynska, R. Aebersold, N. Sonenberg, Hierarchical phosphorylation of the translation inhibitor 4E-BP1. *Genes Dev.* **15**, 2852–2864 (2001).
59. A. C. Gingras, S. P. Gygi, B. Raught, R. D. Polakiewicz, R. T. Abraham, M. F. Hoekstra, R. Aebersold, N. Sonenberg, Regulation of 4E-BP1 phosphorylation: A novel two-step mechanism. *Genes Dev.* **13**, 1422–1437 (1999).
60. L. Hauffe, D. Picard, J. Musa, M. Remke, T. G. P. Grunewald, B. Rotblat, G. Reifenberger, G. Leprivier, Eukaryotic translation initiation factor 4E binding protein 1 (EIF4EBP1) expression in glioblastoma is driven by ETS1- and MYBL2-dependent transcriptional activation. *Cell Death Discov.* **8**, 91 (2022).
61. Y. L. Cha, P. D. Li, L. J. Yuan, M. Y. Zhang, Y. J. Zhang, H. L. Rao, H. Z. Zhang, X. F. Zheng, H. Y. Wang, EIF4EBP1 overexpression is associated with poor survival and disease progression in patients with hepatocellular carcinoma. *PLOS ONE* **10**, e0117493 (2015).
62. N. Tikhmyanova, J. L. Little, E. A. Golemis, CAS proteins in normal and pathological cell growth control. *Cell. Mol. Life Sci.* **67**, 1025–1048 (2010).
63. D. Shahbazian, A. Parsyan, E. Petroulakis, J. Hershey, N. Sonenberg, eIF4B controls survival and proliferation and is regulated by proto-oncogenic signaling pathways. *Cell Cycle* **9**, 4106–4109 (2010).
64. A. G. van Gorp, K. E. van der Vos, A. B. Brenkman, A. Bremer, N. van den Broek, F. Zwartkruis, J. W. Hershey, B. M. Burgering, C. F. Calkhoven, P. J. Coffer, AGC kinases regulate phosphorylation and activation of eukaryotic translation initiation factor 4B. *Oncogene* **28**, 95–106 (2009).
65. L. Simon-Carrasco, G. Jimenez, M. Barbacid, M. Drosten, The Capicua tumor suppressor: A gatekeeper of Ras signaling in development and cancer. *Cell Cycle* **17**, 702–711 (2018).
66. W. Su, H. Hu, Q. Ding, M. Wang, Y. Zhu, Z. Zhang, Z. Geng, S. Lin, P. Zhou, NEK2 promotes the migration and proliferation of ESCC via stabilization of YAP1 by phosphorylation at Thr-143. *Cell Commun. Signal* **20**, 87 (2022).
67. L. M. Simpson, L. J. Fulcher, G. Sathe, A. Brewer, J. F. Zhao, D. R. Squair, J. Crooks, M. Wightman, N. T. Wood, R. Gourlay, J. Varghese, R. F. Soares, G. P. Sapkota, An affinity-directed phosphatase, AdPhosphatase, system for targeted protein *dephosphorylation*. *Chem. Biol.* **30**, 188–202.e6 (2023).
68. H. Zhang, H. Y. Zhao, X. X. Xi, Y. J. Liu, M. Xin, S. Mao, J. J. Zhang, A. X. Lu, S. Q. Zhang, Discovery of potent epidermal growth factor receptor (EGFR) degraders by proteolysis targeting chimera (PROTAC). *Eur. J. Med. Chem.* **189**, 112061 (2020).
69. G. Ahn, S. M. Banik, C. L. Miller, N. M. Riley, J. R. Cochran, C. R. Bertozzi, LYTACs that engage the asialoglycoprotein receptor for targeted protein degradation. *Nat. Chem. Biol.* **17**, 937–946 (2021).
70. A. D. Cotton, D. P. Nguyen, J. A. Gramespacher, I. B. Seiple, J. A. Wells, Development of Antibody-Based PROTACs for the Degradation of the Cell-Surface Immune Checkpoint Protein PD-L1. *J. Am. Chem. Soc.* **143**, 593–598 (2021).
71. Y. Geng, Y. M. Lee, M. Welcker, J. Swanger, A. Zagozdzon, J. D. Winer, J. M. Roberts, P. Kaldis, B. E. Clurman, P. Sicinski, Kinase-independent function of cyclin E. *Mol. Cell* **25**, 127–139 (2007).
72. X. Tan, N. Thapa, Y. Sun, R. A. Anderson, A kinase-independent role for EGF receptor in autophagy initiation. *Cell* **160**, 145–160 (2015).
73. R. A. Fernandes, L. Su, Y. Nishiga, J. Ren, A. M. Bhuiyan, N. Cheng, C. J. Kuo, L. K. Picton, S. Ohtsuki, R. G. Majzner, S. P. Rietberg, C. L. Mackall, Q. Yin, L. R. Ali, X. Yang, C. S. Savvides, J. Sage, M. Dougan, K. C. Garcia, Immune receptor inhibition through enforced phosphatase recruitment. *Nature* **586**, 779–784 (2020).
74. R. Pergu, V. M. Shoba, S. K. Chaudhary, D. N. P. Munkanatta Godage, A. Deb, S. Singha, U. Dhawa, P. Singh, V. Anokhina, S. Singh, S. U. Siriwardena, A. Choudhary, Development and applications of chimera platforms for tyrosine phosphorylation. *ACS Cent. Sci.* **9**, 1558–1566 (2023).

75. Y. Liu, A. Beyer, R. Aebersold, On the dependency of cellular protein levels on mRNA abundance. *Cell* **165**, 535–550 (2016).
76. B. C. Collins, C. L. Hunter, Y. Liu, B. Schilling, G. Rosenberger, S. L. Bader, D. W. Chan, B. W. Gibson, A.-C. Gingras, J. M. Held, M. Hirayama-Kurogi, G. Hou, C. Krisp, B. Larsen, L. Lin, S. Liu, M. P. Molloy, R. L. Moritz, S. Ohtsuki, R. Schlapbach, N. Selevsek, S. N. Thomas, S.-C. Tzeng, H. Zhang, R. Aebersold, Multi-laboratory assessment of reproducibility, qualitative and quantitative performance of SWATH-mass spectrometry. *Nat. Commun.* **8**, 291 (2017).
77. Q. Gao, H. Zhu, L. Dong, W. Shi, R. Chen, Z. Song, C. Huang, J. Li, X. Dong, Y. Zhou, Q. Liu, L. Ma, X. Wang, J. Zhou, Y. Liu, E. Boja, A. I. Robles, W. Ma, P. Wang, Y. Li, L. Ding, B. Wen, B. Zhang, H. Rodriguez, D. Gao, H. Zhou, J. Fan, Integrated Proteogenomic Characterization of HBV-Related Hepatocellular Carcinoma. *Cell* **179**, 561–577.e22 (2019).
78. M. Mehnert, W. Li, C. Wu, B. Salovska, Y. Liu, Combining rapid data independent acquisition and CRISPR gene deletion for studying potential protein functions: A case of HMGN1. *Proteomics* **19**, e1800438 (2019).
79. W. Li, H. Chi, B. Salovska, C. Wu, L. Sun, G. Rosenberger, Y. Liu, Assessing the Relationship between mass window width and retention time scheduling on protein coverage for data-independent acquisition. *J. Am. Soc. Mass Spectrom.* **30**, 1396–1405 (2019).
80. Y. Liu, Y. Mi, T. Mueller, S. Kreibich, E. G. Williams, A. Van Drogen, C. Borel, M. Frank, P.-L. Germain, I. Bludau, M. Mehnert, M. Seifert, M. Emmenlauer, I. Sorg, F. Bezrukov, F. S. Bena, H. Zhou, C. Dehio, G. Testa, J. Saez-Rodriguez, S. E. Antonarakis, W.-D. Hardt, R. Aebersold, Multi-omic measurements of heterogeneity in HeLa cells across laboratories. *Nat. Biotechnol.* **37**, 314–322 (2019).
81. R. Bruderer, O. M. Bernhardt, T. Gandhi, S. M. Miladinovic, L. Y. Cheng, S. Messner, T. Ehrenberger, V. Zanotelli, Y. Butscheid, C. Escher, O. Vitek, O. Rinner, L. Reiter, Extending the limits of quantitative proteome profiling with data-independent acquisition and application to acetaminophen-treated three-dimensional liver microtissues. *Mol. Cell. Proteomics* **14**, 1400–1410 (2015).
82. R. Bruderer, O. M. Bernhardt, T. Gandhi, Y. Xuan, J. Sondermann, M. Schmidt, D. Gomez-Varela, L. Reiter, Optimization of experimental parameters in data-independent mass spectrometry significantly increases depth and reproducibility of results. *Mol. Cell. Proteomics* **16**, 2296–2309 (2017).
83. B. Salovska, H. Zhu, T. Gandhi, M. Frank, W. Li, G. Rosenberger, C. Wu, P.-L. Germain, H. Zhou, Z. Hodny, L. Reiter, Y. Liu, Isoform-resolved correlation analysis between mRNA abundance regulation and protein level degradation. *Mol. Syst. Biol.* **16**, e9170 (2020).
84. E. Gao, W. Li, C. Wu, W. Shao, Y. Di, Y. Liu, Data-independent acquisition-based proteome and phosphoproteome profiling across six melanoma cell lines reveals determinants of proteotypes. *Mol. Omics* **17**, 413–425 (2021).
85. Y. Perez-Riverol, A. Csordas, J. Bai, M. Bernal-Llinares, S. Hewapathirana, D. J. Kundu, A. Inuganti, J. Griss, G. Mayer, M. Eisenacher, E. Perez, J. Uszkoreit, J. Pfeuffer, T. Sachsenberg, S. Yilmaz, S. Tiwary, J. Cox, E. Audain, M. Walzer, A. F. Jarnuczak, T. Ternent, A. Brazma, J. A. Vizcaino, The PRIDE database and related tools and resources in 2019: Improving support for quantification data. *Nucleic Acids Res.* **47**, D442–D450 (2019).

Acknowledgments: We acknowledge critical discussion from members of the C.M.S. Laboratory: S. Jaime-Figueroa, K. Li, T. Douglas, and C. De Leon. We acknowledge S. Zhou from Center for Excellence in Molecular Cell Science, CAS for assistance with MS. **Funding:** This study was supported by NIH R35 CA197589 and an American Cancer Society Research Professorship (RP-18-210-01-CDD) to C.M.C., NIH grant R01GM137031 to Y.L., Shanghai Pujiang Program to Z.H., and National Science and Technology Council in Taiwan (NSTC111-2628-B-006-024, 112-2628-B-006-007) to P.-H.C. This study does not reflect the sponsor's position or the policy of the government, and no official endorsement was inferred. **Author contributions:** Z.H., P.-H.C., and C.M.C. designed the experiments with helpful input from S.Z., J.S., and W.L. Z.H., P.-H.C., M.K., S.Z., J.S., and I.U.V. performed the experiments. M.K. supervised the SPR study. W.L. performed and supervised proteomic study. Y.L. supervised and managed the proteomic study. C.M.C. supervised and managed the project. J.H. edited the manuscript and provided critical suggestions. Z.H. and P.-H.C. wrote the manuscript. All authors read, edited, and approved the manuscript. Z.H., P.-H.C., and W.L. contributed equally to this work. **Competing interests:** The authors declare that they have no competing interests. **Data and materials availability:** All data needed to evaluate the conclusions in the paper are present in the paper and/or the Supplementary Materials.

Submitted 16 July 2023
Accepted 22 February 2024
Published 27 March 2024
10.1126/sciadv.adj7251